MERIS 3rd data reprocessing

Software and ADF updates

Ref.: A879.NT.008.ACRI-ST

Issue: 1.0

Date: 27/06/2011

Contract N°: 21091/07/I-OL

Preparation and signature list

	Name and role	Company	Signature
Prepared by the MERIS QWG members	Ludovic Bourg	ACRI-ST	
	Christophe Lerebourg, Editor	ACRI-ST	
	Constant Mazeran	ACRI-ST	
	Véronique Bruniquel, Editor	ACRI-ST	
	Kathryn Barker	ARGANS	
	Jan Jackson	ARGANS	
	Christopher Kent	ARGANS	
	Samantha Lavender	ARGANS	
	Gerald Moore	Bio-Optika	
	Carsten Brockmann	Brockmann Consult	
	Marc Bouvet	ESA	
	Steven Delwart	ESA	
	Philippe Goryl	ESA	
	Jean-Paul Huot	ESA	
	Ewa Kwiatkowska	ESA	
	Jürgen Fisher	FUB	
	Didier Ramon	Hygeos	
	Roland Doerffer	HZG	
	David Antoine	LOV	
	Francis Zagolski	Parbleu	
	Richard Santer	ULCO	
Approved by	Odile Fanton d'Andon, Managing Director	ACRI-ST	
Authorised by	Philippe Goryl	ESA	

Distribution List

To	Company
Philippe Goryl	ESA
+ Public distribution	

Version History

Version	Date	Changes
1.0	27/06/2011	First version

Table of Content

List of Figures

List of Tables

Acknowledgement to *in situ* data contributors

A large part of the MERIS 3rd reprocessing over the Ocean has been possible thanks to *in situ* measurements, which constitute essential independent reference data to calibrate and validate the algorithms.

The MERIS Quality Working Group is greatly grateful to all the scientists and associated laboratories who share their datasets within **MERMAID**, the validation facility used to extract MERIS matchups.

The **MERMAID** website http://hermes.acri.fr/mermaid contains details about the datasets, email contact and a protocol measurements document for all available datasets (*MERIS Optical Measurement Protocols - Part A: In situ water reflectance measurements*).

In particular, the MERIS Quality Working Group thanks the following Principle Investigators and mission responsibles who currently contribute to the MERIS validation:

- **Giuseppe Zibordi** (Joint Research Center, Italy) for providing data at four AERONET- OC sites: the Acqua Alta Oceanographic Tower, Abu Al Bukhoosh, Gustav Dalen Tower and Helsinki Lighthouse.
  - G. Zibordi, B. Holben, I. Slutsker, D. Giles, D. D'Alimonte, F. Mélin, J.-F. Berthon, D. Vandemark, H. Feng, G. Schuster, B. Fabbri, S. Kaitala, J. Seppälä. AERONET-OC: a network for the validation of Ocean Color primary radiometric products. Journal of Atmospheric and Oceanic Technology, 26, 1634-1651, 2009.
  - G.Zibordi, J.-F.Berthon, F.Mélin, D. D'Alimonte and S.Kaitala. Validation of satellite ocean color primary products at optically complex coastal sites: northern Adriatic Sea, northern Baltic Proper and Gulf of Finland. Remote Sensing of Environment, 113, 2574-2591, 2009.
- **John Icely** (University of Algarve, Portugal) for the Sagres coast dataset.
  - Cristina, S., Goela, P., Icely, J. I., Newton, A. & Fragoso, B. (2009). Assessment of water-leaving reflectance of the oceanic and coastal waters using MERIS satellite products off the southwest coast of Portugal. *Journal of Coastal Research* Special Issue (56): 5.

Acknowledgement to *in situ* data contributors (*cont.*)

- **David Antoine** (Laboratoire d'Océanographie de Villefranche, France) for the BOUSSOLE dataset, used in particular for the vicarious adjustment.
  - Antoine, D. M. Chami, H. Claustre, F. D'Ortenzio, A. Morel, G. Bécu, B. Gentili, F. Louis, J. Ras, E. Roussier, A.J. Scott, D. Tailliez, S. B. Hooker, P. Guevel, J.-F. Desté, C. Dempsey and D. Adams. 2006, BOUSSOLE : a joint CNRS-INSU, ESA, CNES and NASA Ocean Color Calibration And Validation Activity. NASA Technical memorandum N° 2006 – 214147.
  - Antoine, D., P. Guevel, J.-F. Desté, G. Bécu, F. Louis, A. J. Scott and P. Bardey, 2008, The «BOUSSOLE» buoy A new transparent-to-swell taut mooring dedicated to marine optics: design, tests and performance at sea, *Journal of Atmospheric and Oceanic Technology*, 25, 968-989.
- **David McKee** (University of Strathclyde, UK) for the Bristol Channel and Irish Sea datasets.
- **Mati Kahru** (University of California, US) for the California Current dataset.
- **Hubert Loisel** (Laboratoire d'Océanologie et de Géosciences, France) for the East English Channel and French Guiana datasets.
  - **H. Loisel**, X. Mériaux, A. Poteau, L. F. Artigas, B. Lubac, A. Gardel, J. Caillaud, and S. Lesourd, 2007, Analyze of the inherent optical properties of French Guiana coastal waters for remote sensing applications. Journal of Coastal Research SI 56 (Proceedings of the 10th International Coastal Symposium), 1532 – 1536.
  - B. Lubac and **H. Loisel**, 2007, Variability and classification of remote sensing reflectance spectra in the Eastern English Channel and southern North Sea. Remote Sensing of Environment 110, 45-58.
- **Michael Ondrusek** (NOAA) for the MOBY dataset used for the vicarious adjustment.
  - Clark, D. K., Yarborough, M. A., Feinholz, M. E., Flora, S., Broenkow, W., Kim, Y. S., Johnson, B. C., Brown, S. W., Yuen, M. & Mueller, J. L. (2003).MOBY, A Radiometric Buoy for Performance Monitoring and Vicarious Calibration of Satellite Ocean Colour Sensors: Measurements and Data Analysis Protocols. In Ocean Optics Protocols for Satellite Ocean Colour Sensor Validation, NASA Technical Memo. 2003-211621/Rev4, Vol VI, 3-34 (Eds J. L. Muller, G. Fargion and C. McClain). Greenbelt, MD.: NASA/GSFC.
- **Kevin Ruddick** (MUMM, Belgium) for the MUMMTriOS dataset.
  - Ruddick, K. G., V. De Cauwer, Y. Park and G. Moore (2006). Seaborne measurements of near infrared water-leaving reflectance - the similarity spectrum for turbid waters. Limnology and Oceanography 51(2): 1167-1179.

Acknowledgement to *in situ* data contributors (*cont.*)

- **Doug Vandemark** and **Hui Feng** (University of New Hampshire, US) for the AERONET-OC MVCO dataset.
  - G. Zibordi, B. Holben, I. Slutsker, D. Giles, D. D'Alimonte, F. Mélin, J.-F. Berthon, D. Vandemark, H. Feng, G. Schuster, B. Fabbri, S. Kaitala, J. Seppälä. AERONET-OC: a network for the validation of Ocean Color primary radiometric products. *Journal of Atmospheric and Oceanic Technology*, 26, 1634-1651, 2009.
- **Jeremy Werdell** (NASA), **Larry Harding** (University of Maryland, US), **Antonio Mannino** (NASA), **Ajit Subramaniam** (University of Maryland, US), **Dariusz Stramski** (University of California, US), **Greg Mitchell** (University of California, US), **William Balch** (Bigelow Laboratory for Ocean Sciences, US), **Frank Muller-Karger** (University South Florida, US), **Ru Morrison** (Woods Hole Oceanographic Institution, US), **Zhongping Lee** (Naval Research Laboratory), **Ken Carder** (Professor Emeritus University South Florida, US), **Norman Nelson** (University of California, US), **Richard Gould** (Naval Research Laboratory, US), **Robert Arnone** (Naval Research Laboratory, US) and **Stan Hooker** (NASA) for the NOMAD dataset.
  - Werdell, P.J. and S.W. Bailey, 2005: An improved bio-optical data set for ocean color algorithm development and satellite data product validation. *Remote Sensing of Environment*, 98(1), 122-140.
- **Suzanne Kratzer** (University of Stockholm, Sweden) for the North-Western Baltic Sea and AERONET-OC Palgrunden dataset.
  - Kratzer, S., Brockmann, C. & Moore, G. F. (2008). Using MERIS full resolution data (300 m spatial resolution) to monitor coastal waters– a case study from Himmerfjärden, a fjord-like bay in the north-western Baltic Sea. Remote Sensing of the Environment 112(5): 2284-2300.
- **David Siegel** (University of California, US) for the Plumes and Blooms dataset.
- **Pierre-Yves Deschamps** (Laboratoire d'Optique Appliquée, France) for the SIMBADA dataset.
- **Annelies Hommersom** (IVM, Netherlands) for the Wadden Sea dataset.

1 Introduction

1.1 Scope of the document

This document prepared by the MERIS Quality Working Group (QWG) aims at compiling and presenting all Level 1 and Level 2 evolutions implemented in the 3rd MERIS data reprocessing, in term of algorithm and Auxiliary Data File (ADF) changes.

Algorithms and configuration correspond to version 8.0 of the MERIS Ground Segment prototype (MEGS), delivered to the whole community through the ODESA software. It is equivalent to version 6.0 of the Instrument Processing Facilities (IPF) at ESRIN.

The list of changes described in this document is exhaustive. However, full details on algorithms and validation should be read in publications referenced at the end of each section.

Furthermore, this document does not describe algorithms or auxiliary data which have not encountered any change since the 2nd reprocessing.

A future version of this document, to be issued, will present accuracy of the products.

1.2 Structure of the document

This document is split into the following chapters:

- This chapter introduces the document;
- **Chapter 2 – Reprocessing overview**, summarises the 3rd reprocessing evolutions with associated list of documentation;
- **Chapter 3 – Level 1 data processing**, details the MERIS Level 1 products and algorithms evolutions;
- **Chapter 4 – Level 2 data processing – Common branch**, details the MERIS Level 2 products/flags and algorithms evolutions for the common processing branch;
- **Chapter 5 – Level 2 data processing – Cloud branch**, details the MERIS Level 2 products/flags and algorithms evolutions for the cloud processing branch;
- **Chapter 6 – Level 2 data processing – Ocean branch**, details the MERIS Level 2 products/flags and algorithms evolutions for the ocean processing branch;
- **Chapter 7 – Level 2 data processing – Land branch**, details the MERIS Level 2 products/flags and algorithms evolutions for the land processing branch;

1.3 Acronyms

The definition of the acronyms used in this document is listed below:

AC	Atmospheric Correction
AD	Applicable Document
ADF	Auxiliary Data File
AMORGOS	Accurate MERIS Ortho-Geolocation Operational Software
AOT	Aerosol Optical Thickness
ARVI	Atmospherically Resistant Vegetation Index
ASH	Aerosol Scale Height
ATBD	Algorithm Theoretical Basis Document
BEAM	Basic ERS and Envisat (A)ATSR and MERIS Toolbox
BENCAL	BENGUELA current, MERIS-MODIS-SeaWiFS inter-calibration cruise
BIOSOPE	BIogeochmistry and Optics South Pacific Experiment
BOUSSOLE	BOUée pour l'acquiSition de Séries Optiques à Long Terme
BPAC	Bright Pixel Atmospheric Correction
CTP	Cloud Top Pressure
CZCS	Coastal Zone Color Scanner
DDV	Dense Dark Vegetation
DEM	Digital Elevation Model
ECMWF	European Centre for Medium-Range Weather Forecast
EO	Earth Observation
ESA	European Space Agency
ESFT	Exponential Sum Fitting Technique
FR	Full Resolution
GAME	Global Absorbing ModEl
GPS	Global Positioning System
FAPAR	Fraction of Absorbed Photosynthetically Active Radiation
FOV	Field Of View
FUB	Freie Universität Berlin
GOME	Global Ozone Monitoring Experiment
HITRAN2000	High Resolution Transmission
HZG	Helmholtz-Zentrum Geesthacht
ICOL	Improved Contrast between Ocean and Land (adjacency effect correction)
IOCCG	International Ocean Colour Coordinating Group
IOP	Inherent Optical Properties
IPF	Instrument Processing Facilities

L1, L2, L3	Level 1, Level 2, Level 3
LARS	Land Aerosol Remote Sensing
LBL	Line-By-Line
LOV	Laboratoire Océanologique de Villefranche-Sur-Mer
LUT	Look-Up Table
MBR	Maximum Band Ratio
MDS	MERIS Data Set
MDSI	MERIS Differential Snow Index
MEGS	MERIS processing chain prototype
MERIS	Medium Resolution Imaging Spectrometer
MERMAID	MERIS MAtchup In situ database
MGVI	MERIS Global Vegetation Index
MOBY	Marine Optical Buoy
MODIS	Moderate Resolution Imaging Spectrometer
MOMO	Matrix Operator MethOd
MWR	Microwave Radiometer
NIR	Near Infra-Red
NN	Neural Network
NOMAD	NASA Bio-Optical Marine Algorithm Data Set
OC4v4	4-band Ocean Colour Chlorophyll algorithm, version 4
ODESA	Optical Data processor of the European Space Agency
PCD	Product Confidence Data
QWG	Quality Working Group
RMS	Root Mean Square Error
RPD	Relative Percent Difference
RR	Reduced Resolution
SAM	Standard Aerosol Model
SIO	South Indian Ocean
SOS	Successive Orders of Scattering
SPG	South Pacific Gyre
RD	Reference Document
RTC	Radiative Transfert Code
SAM	Standard Aerosol Model
SeaWiFS	Sea-Viewing Wide Field of View Sensor
SIMBADA	In situ dataset measured from the SIMBADA radiometer
SWIR	Short –Wave Infrared
SZA	Solar Zenith Angle
TOA	Top Of Atmosphere

TSM	Total Suspended Matter
ULCO	Université du Littoral et de la Côte d'Opale
VIS	Visible
VZA	View Zenith Angle
WGS	World Geodetic System
YS	Yellow Substance

2 Overview of the 3rd reprocessing

2.1 History of the MERIS data reprocessings

Data reprocessings are required to improve the archived products. They are planned by the MERIS QWG in order to address known issues, and consequently to improve algorithms and auxiliary tables involved in the MERIS data processing.

Before the current reprocessing which ends in March 2011, two previous ones took place in 2004 and 2005. Details on changes and data quality assessment can be founded in the ENVISAT website document at http://earth.eo.esa.int/pcs/envisat/meris/documentation:

Reprocessing 1 – 2004

Description document: First_2003_MERIS_Reprocessing.pdf

Quality assessment document: MERISQualityAssessment-MEGS7-QWG-V1.pdf

MEGS version: 7.0

IPF version: N/A

Time range of processing: whole year 2003

Reprocessing 2 – 2005

Description document: MERISRRsecondreprocessing-V2.pdf

Quality assessment document: MERISQualityAssessment-MEGS74-IPF502-QWG-V1.0.pdf

MEGS version: 7.0

IPF version: 5

Time range of processing: April 2002 to present (until installation of IPF 6, IPF 5 is still used in operational NRT processing)

Reprocessing 3 – 2011

Description document: chapter 2 to 7 of the present document

Quality assessment document: to be issued in 2011

MEGS version: 8.0

IPF version: 6

Time range of processing: from April 2002 on.

2.2 Overview of the 3rd MERIS data reprocessing

Both Level 1 and Level 2 products are impacted by the 3rd reprocessing.

- A new calibration and improved geolocation impacts the Level 1 products in term of radiometry, geometry and flags for land/ocean/coastline classification (see Table 1);
- The most important evolution of the 3rd reprocessing refers to Level 2 changes (see Table 2 for impact on products and Table 3 for impact on flags). It impacts individually all branches (cloud, land and ocean) as well as the common branch (gaseous correction). Note also that all Level 2 products will be affected by the Level 1 new calibration.

A synthetic description of 2nd reprocessing known issues, 3rd reprocessing solutions and 3rd reprocessing impacts on products and flags is presented in:

- Table 4 for L1 data processing;
- Table 5 for L2 data processing – Common branch;
- Table 6 for L2 data processing – Cloud branch;
- Table 7 for L2 data processing – Land branch;
- Table 8 and Table 9 data processing – Ocean branch.

For more readability, these tables are also available in a separated document considered as an appendix of this report.

Table 1: Impact of the 3rd data reprocessing on Level 1 products and flags – Grey lines correspond to not impacted products or flags.

		Processing	Product name	Changed for 3rd reprocessing	Nature of change	ATBD	section in DPM 8.0	Details in §
MERIS Level 1	Product	Radiometric processing	Top Of the Atmosphere Radiances (x15)	Yes	V	N/A	6	3.1 & 3.2
		N/A	*Detector Index*	*No*	*N/A*	*N/A*	*N/A*	*N/A*
		Geo-location Processing Algorithms	latitude	YES	V	N/A	8	3.2
			longitude					
			DEM altitude					
			DRM roughness					
			DEM latitude correction					
			DEM longitude correction					
			sun zenith angle					
			sun azimuth angle					
			viewing zenith angle					
			viewing azimuth angle					
		External data assimilation	*zonal wind*	*No*	*N/A*	*N/A*	*10*	*N/A*
			meridional wind					
			mean sea level pressure					
			ozone					
			relative humidity					
	Flag	*Saturated pixel detection*	*invalid*	*No*	*N/A*	*N/A*	*5*	*N/A*
		Radiometric processing	*cosmetic*	*No*			*6*	
		Geo-location Processing Algorithms	*duplicated*	*No*			*8*	
			glint risk	*No*				
		Pixel classification	land (1) ; ocean (0)	yes	V	*N/A*	9	3.2
			bright	*No*	*N/A*	*N/A*	*9*	*N/A*
			coastline	yes	V	*N/A*	9	3.2
		Product formatting	*suspect*	*No*	*N/A*	*N/A*	*11*	*N/A*

**A=Algorithmic, F=Format of ADF, V=Value in ADF

Table 2: Impact of the 3rd data reprocessing on Level 2 products – Grey lines correspond to not impacted products

		Processing	Product name	Changed for 3rd reprocessing	Nature of change	ATBD	section in DPM 8.0a	Details in §
MERIS Level 2	Products	Ocean Products	Water Leaving Reflectance	Yes	A + F	2.6. 2.7.2.11	8.3;8.4	6.1-5
			Algal Pigment Index I	Yes	A + F	2.9	8,5	6,6
			Algal Pigment Index II	Yes	A	2.12	8.6	6.7
			Total Suspended Matter	Yes	A	2.12	8.6	6.7
			Yellow substance	Yes	A	2.12	8.6	6.7
			Photosynthetically Active Radiation (PAR)	*No*	*N/A*	*2.18*	*8.5*	*N/A*
			Aerosol optical thickness (443, 550, 865)	Yes	A + F	2.7	8.4	6.1-5
			Water Vapour	*No*	*N/A*	*2.4*	*6*	*N/A*
			Aerosol Angström Coefficient	Yes	A + F	2.7	8.4	6.1-5
		Cloud products	*Cloud optical thickness*	*No*	*N/A*	*2.1*	*7*	*N/A*
			Cloud albedo	*No*	*N/A*	*2.2*	*7*	*N/A*
			Cloud Top Pressure	Yes	V	2.3	4	5.1
			Cloud Type	*No*	*N/A*	*N/A*	*7*	*N/A*
			Cloud reflectance (not applicable; reflectance over cloud are TOA reflectance)	*No*	*N/A*	*N/A*	*7*	*N/A*
		Land products	Surface Reflectance	Yes	A + F	2.15	9.3	7.2
			Aerosol optical thickness	Yes	A + F	2.15	9.3	7.2
			Aerosol Angström Coefficient	Yes	A + F	2.15	9.3	7.2
			MGVI - Meris Global Vegetation Index - TOA vegetation Index - FAPAR	Yes	A + F	2.10	9.2	7.4
			MTCI - Meris Terrestrial Chlorophyll Index -BOA vegetation index	*No*	*N/A*	*2.1*	*9.4*	*N/A*
			surface pressure	Yes	A + F	2.23	4	7.3
			Water Vapour	Yes	A + F	2.4	6	7.1

*all level 2 products are affected by Common Branch evolutions (Not considered in this table)
**A=Algorithmic, F=Format of ADF, V=Value in ADF

Table 3: Impact of the 3rd data reprocessing on Level 2 flags – Grey lines correspond to not impacted flags

MERIS Level 2 — Flags

Processing	Product name		Changed for 3rd reprocessing	Nature of change	ATBD	section in DPM 8.0a	Details in §
Surface classification	LAND		Yes	A	2.17	5	4.2
	CLOUD		Yes	A	2.17	5	4.2
	WATER		Yes	A	2.17	5	4.2
Product confidence	PCD_1_13	- confidence flag for water leaving/surface reflectanc	Yes	V	N/A	10.5.13	6.12-13
	PCD_14	*- confidence flag for water vapour*	*No*	*N/A*	*N/A*	*10.5.13*	*N/A*
	PCD_15	*- confidence flag for algal pigment index 1 / MGVI / CTP*	*No*	*N/A*	*N/A*	*10.5.13*	*N/A*
	PCD_16	- confidence flag for YS or TSM / rectified reflectance	Yes	A	N/A	10.5.13	6.14
	PCD_17	- confidence flag for algal pigment index 2 / MTCI	Yes	A	N/A	10.5.13	6.14
	PCD_18	*- confidence flag for PAR/Land surface pressure/cloud albedo*	*No*	*N/A*	*N/A*	*10.5.13*	*N/A*
	PCD_19	*- confidence flag for aerosol type and optical thickness / COT*	*No*	*N/A*	*N/A*	*10.5.13*	*N/A*
Science flags	COASTLINE	- from Level 1b	Yes		N/A	10.5.13	3.1
	COSMETIC	*- from Level 1b*	*No*	*N/A*	*N/A*	*10.5.13*	*N/A*
	SUSPECT	*- from Level 1b*	*No*	*N/A*	*N/A*	*10.5.13*	*N/A*
	OADB	- Out Of Aerosol model DataBase:no braketing aerosol found	*No*	*N/A*	*N/A*	10.5.13	6.4
	ABSOA_DUST	- Desert dust absorbing aerosol/Continental absorbing aerosol	*No*	*N/A*	*N/A*	10.5.13	6.4
	CASE2_S	- Case 2 sediment dominated waters / Turbid water	Yes	A	N/A	10.5.13	6.3
	CASE2_ANOM	- Anomalous scattering water	Yes	V	N/A	10.5.13	6.12
	CASE2_Y	*- Yellow substance loaded water*	*No*	*N/A*	*N/A*	*10.5.13*	*N/A*
	ICE_HAZE	- ice or high aerosol load	Yes	A	N/A	10.5.13	6.9
	MEDIUM_GLINT	*- Medium Glint reflectance correction applied*	*No*	*N/A*	*N/A*	*10.5.13*	*N/A*
	BPAC_ON	- Bright Pixel Atmospheric Correction	Yes	A	N/A	10.5.13	6.10
	HIGH_GLINT	*- no glint correction applied*	*No*	*N/A*	*N/A*	*10.5.13*	*N/A*
	LOW_SUN	*- low sun angle*	*No*	*N/A*	*N/A*	*10.5.13*	*N/A*
	WHITE_SCATTERER	*- white scatterers within water*	*No*	*N/A*	*N/A*	*10.5.13*	*N/A*
	TOAVI_BRIGHT	*- Bright flag from TOAVI spectral tests*	*No*	*N/A*	*N/A*	*10.5.13*	*N/A*
	TOAVI_BAD	*- Bad data from TOAVI spectral tests*	*No*	*N/A*	*N/A*	*10.5.13*	*N/A*
	TOAVI_CSI	*- Cloud, snow or ice from TOAVI spectral tests*	*No*	*N/A*	*N/A*	*10.5.13*	*N/A*
	TOAVI_WS	*- water or deep shadow from TOAVI spectral tests*	*No*	*N/A*	*N/A*	*10.5.13*	*N/A*

*all level 2 products are affected by Common Branch evolutions (Not considered in this table)
**A=Algorithmic, F=Format of ADF, V=Value in ADF

Table 4: Details of the 3rd reprocessing changes in L1 data processing

Processing step	Concerned product /algorithm	2nd reprocessing know issues	3rd reprocessing solutions	3rd reprocessing impact
L1 data processing				
L1 data processing	Geolocation	Not prepared to take into account elevation in geolocation (Ortho-geo-referencing)	Nature of instrument pointing auxiliary data has been updated to include full direction cosines at every pixel	Slight geolocation differences can be observed.
	L1 calibration	Model uses on board calibration up to 20041103	Include latest on board calibration in the model	Improve radiometric stability with time, pixel to pixel stability and camera interface continuity

Table 5: Details of the 3rd reprocessing changes in L2 data processing – Common branch

Processing step	Concerned product /algorithm	2nd reprocessing know issues	3rd reprocessing solutions	3rd reprocessing impact
L2 data processing – Common branch				
Gaseous correction	O2 transmission correction	Degraded O2 transmittance correction leading to errors in atmospheric correction, due to the location of the MERIS band 12 at the long-wave end of the Oxygen-A absorption band	Calculation of the O2 transmission based on a 5-D interpolation of MOMO RT LUT values. The 5 variables are the central wavelength of band 12, the mormalised measured radiance, the solar and viewing zenith and azimuth directions.	Improvement of atmospheric correction and all procedures using MERIS band 12 Less noise of the retrieved products
	H2O transmission correction	N/A	Introduction of a molecular depolarisation factor	A maximum of 1% relative absolute difference in TOA reflectance for H2O corrected bands
	O3 transmission correction	Outdated LUT	O3 transmittance LUT has been refreshed using a better spectral integration	negligeable impact on TOA reflectance gaz correction
Pixel classification	Identification of Cloud pixel over Water	Over water, too few cloudy pixels were detected (cloud borders, less bright scattered clouds and thin clouds)	Additional threshold tests (+ 1 bright reflectance test and 1 pressure test) followed by a snow/ice test have been introduced in order to detect more cloudy pixels and discriminate snowy/ice pixels from clouds.	More pixels classified as cloud Cloud borders, less bright scattered clouds and thin clouds identified as cloud
	Identification of Cloud pixel over Land	Over Land, insufficient cloud detection (less bright or optically thin clouds; insufficient bright land, snow and ice discrimination from clouds.	Remove of the spectral slope tests and apply of a new dedicated ice/snow test. Additional test on apparent height of the scattered surface	More pixels classified as cloud
	Identification of Snow and ice pixel	Snow and ice pixels classified as cloud pixels	Adding of a threshold test on MDSI applied on bright pixels over land and water.	Improvement of the classification between snow/ice pixels from cloud pixel

Table 6: Details of the 3rd reprocessing changes in L2 data processing – Cloud branch

Processing step	Concerned product /algorithm	2nd reprocessing know issues	3rd reprocessing solutions	3rd reprocessing impact
L2 data processing – Cloud branch				
Cloud top pressure	Cloud top pressure	Prominent camera boundaries along MERIS swath with cloud top pressure jumps up to 50 hPa due to stray light	Derivation of an empirical stray light correction from a new surface pressure algorithm, a DEM and the use of ECMWF surface pressure values. Surface albedo is now derived from MERIS data and at 0.05°x0.05° spatial resolution Improved input data values for the cloud top pressure algorithm based on NN approach	Significant reduction of camera boundary jumps More accurate and consistent cloud top pressure along the full MERIS swath

Table 7: Details of the 3rd reprocessing changes in L2 data processing – Land branch

Processing step	Concerned product /algorithm	2nd reprocessing know issues	3rd reprocessing solutions	3rd reprocessing impact
L2 data processing – Land branch				
Water vapour	Water vapour	Impact of the spectral slope on the surface albedo neglected to retrieve water vapour	New water vapour algorithm based on the inversion of MOMO RT simulations using Neural Network technique	Accuracy of the WV significantly improved
LARS	AOT(440) and Angstöm exponent between 440 and 670 nm over Dense Vegetation pixel	Poor quality of Angström retrieval	Implementation of a two band retrieval method Regeneration of the LARS reflectance LUT using MERIS Albedo Map project outputs	Improvement of the Angström exponent retrieval Improvement of the aerosol retrieval spatial coverage
Surface pressure	Surface pressure	Prominent camera boundaries along the MERIS swath with surface pressure product	An empirical stray light correction derived from a new surface pressure algorithm	The surface pressure product is more consistent and accurate in
fAPAR	fAPAR/MGVI	No product over none vegetated aeras	Dedicated set of parameter introduced to compute rectified reflectance over none vegetated aera	No impact where FAPAR computation succeed. product over bright soil not identified as cloud or ice
Flag	Flag SNOW	Need to improve snow/ice detection	A test for snow and ice using the MERIS Differential Snow Index (MDSI) has been introduced in the pixel classification processing	Better differenciation of cloud and snow/ice

Table 8: Details of the 3rd reprocessing changes in L2 data processing – Ocean branch (products)

Processing step	Concerned product /algorithm	2nd reprocessing know issues	3rd reprocessing solutions	3rd reprocessing impact
L2 data processing – Ocean branch				
Smile correction	TOA reflectance	Not optimal wavelength interpolation at central band over ocean	Improved interpolation for the Rayleigh contribution	Very small impact on TOA reflectance and further products
Input of Atmospheric Correction	Vicarious adjustment	Overestimation of MERIS water leaving reflectance compared with in-situ measurements	NIR and VIS vicarious adjustment. Inlusion of vicarious spectral gains in the Ocean Aerosol ADF	Significant reduction of the water leaving reflectance bias
Bright pixel Atmospheric Correction	Whole Bright Pixel Atmospheric Correction algorithm	Poor performances on highly turbid waters. returned 0.0 on failure	Procedure fully revised. Algorithm defined in terms of IOPS, variation of f/Q accounted for, tests on band 885	Improve performances over very turbid waters. Returns pure water signal on failure, applied everywhere
Atmospheric correction	Rayleigh LUT and interpolation	Poor discretisation of wind speed and angle in the RT LUT, polarisation not taken into account	Inclusion of polarisation in RT computation, 3 wind speed instead of 2, cosine interpolation	Bias removal of molecular and fresnel reflection polarisation of up to 3% at 865nm. 3 wind speed reduce extrapolation discrepencies for higher wind speed
	Aerosol LUT and interpolation	Unsatisfying set of blue aerosols,poor discretisation of wind speed and angle in the RT LUT	LUT generated for a set of 6 AOT(550), 3 wind speed, instead of respectively 5, 2. Gauss angle distribution and cosine interpolation implemented. Same aerosol models (16 SAM +18 DUST) except for 3 IOPA insted of 3 blue models	Better retrival of aerosol reflectance
	Transmittance LUT and interpolation	Approximated by an analytical formulation	Introduce LUT for upward and downward transmittances instead of Gordon & Wang formulas	Better retrieval of diffuse transmittance
	Marine reflectance in the NIR	Null or pure water reflectance?	Water leaving reflectance at bands 779, 865 and 885 nm are now the output of the BPAC (corrected for transmittance)	More realistic values of water leaving reflectance in the NIR
Algal pigment index retrieval	OC4Me	The procedure to develop the bio-optical model lack of both very low and very high in situ chl concentration. Use threshold for band ratio selection	Incorporate BIOSOPE and BENCAL in situ data in the model. Use maximum band ratio	Produce lower Chl for low values and slightly higher Chl values in the upper part of the Chl range
	f/Q table with Raman	Outdated parametrization of the bidirectionality	Using the latest parameterization of the bidirectionality, including Raman scattering and a Chl-varying volume scattering phase function	No major impact expected
Case 2 products (chl2, yellow substances, total suspended matter)	Case 2 regional Neural Network	A marine Neural network (NN) used to compute Case 2 products using water leaving reflectance from the standard atmospheric correction	An additional NN now performs atmospheric correction, also followed by a new marine NN.	Improved coverage and reduced noise of Case 2 products

Table 9: Details of the 3rd reprocessing changes in L2 data processing – Ocean branch (flags)

Processing step	Concerned product /algorithm	2nd reprocessing know issues	3rd reprocessing solutions	3rd reprocessing impact
L2 data processing – Ocean branch				
Science/confidence Flags	Flag PCD_1_13	Vicarious adjutment drives water leaving reflectance towards zero in the red and NIR over clear waters	Introduce a threshold to accept slightly negative water leaving reflectances interpreted as noise around zero	Reduce noise impact on valid water-leaving reflectance
	Flag PCD_16	Need to update definition because of additional NN atmospheric correction	Checks on out of scope atmospheric and marine NN outputs	PCD_16 almost never raised because threshold for triggering it is too relaxed
	Flag PCD_17	Need to update definition because of additional NN atmospheric correction	Checks on out of scope atmospheric and marine NN outputs (same as PCD_16)	PCD_17 almost never raised because threshold for triggering it is too relaxed
	Flag CASE_2Anom	AC anomaly at high scattering angles trigers CASE_2ANOM even in open ocean	Adapt thesholds to raise flag	Reduce spatial coverage of case2_anom
	Flag BPAC_ON	Flag always raised	BPAC_ON means BPAC is successful and produces an output different from pure-water	Improve understanding of BPAC
	Flag ICE_HAZE	No sea ice detection	New definition depending on high glint, medium glint, bright test, MDSI and white_scatterer.	Reduction of ICE_HAZE flagged pixels

3 Level 1 data processing

3.1 Level 1 calibration

Contributors: Ludovic Bourg (ACRI-ST) and Christophe Lerebourg (ACRI-ST)

Purpose and description of changes

MERIS is a self calibrating instrument thanks to on-board solar diffusers of characterised reflectivity periodically deployed in the instrument light path. These measurements allow absolute radiometric calibration of the instrument and accurate monitoring of its evolution with time. Since 2nd re-processing, calibration coefficients used routinely in the Earth Observation (EO) Level 0 to Level 1b processing are implemented via absolute radiometric gains at a reference time and a model of their evolution with time. The version of this set of parameters used for the second re-processing was derived from all the available radiometric calibration data acquired in flight up to orbit 14000 (20041103). It is referred in what follows to the 2004 model. It has been kept in use continuously since then to maintain radiometric consistency but has shown limitations in time extrapolation. It was thus decided to derive a new model for 3rd reprocessing using expanded data set.

In addition, some of the assumptions or options chosen to derive the 2004 model were judged irrelevant with increasing ageing of the instrument. The goals behind the derivation of new model parameters and improved methodology are the following:

- Account for instrument sensitivity loss including in the Near InfraRed (NIR), previously assumed stable but proven to have degraded by about 0.5% after 7 years of mission;
- Improve overall radiometric stability with time;
- Improve pixel to pixel homogeneity, including in terms of relative spectral consistency (band ratios);
- Improve continuity at camera interfaces, in particular in terms of temporal stability.

Impact, expected change on product

Figure 1 shows estimates of pixel to pixel variability at beginning of mission, on the one hand, and of its stability with time, on the other hand, for both 2nd and 3rd reprocessing Level 1b.

These estimates have been obtained from very homogeneous areas over Antarctica, as presented in Figure 1. Those results show that both pixel to pixel variability and its time stability are significantly improved for 3rd reprocessing data. Camera interfaces are highlighted in pixel to pixel variability at beginning of mission in 3rd re-processing data but remain stable with time, so that the overall match is still improved when the whole mission is considered.

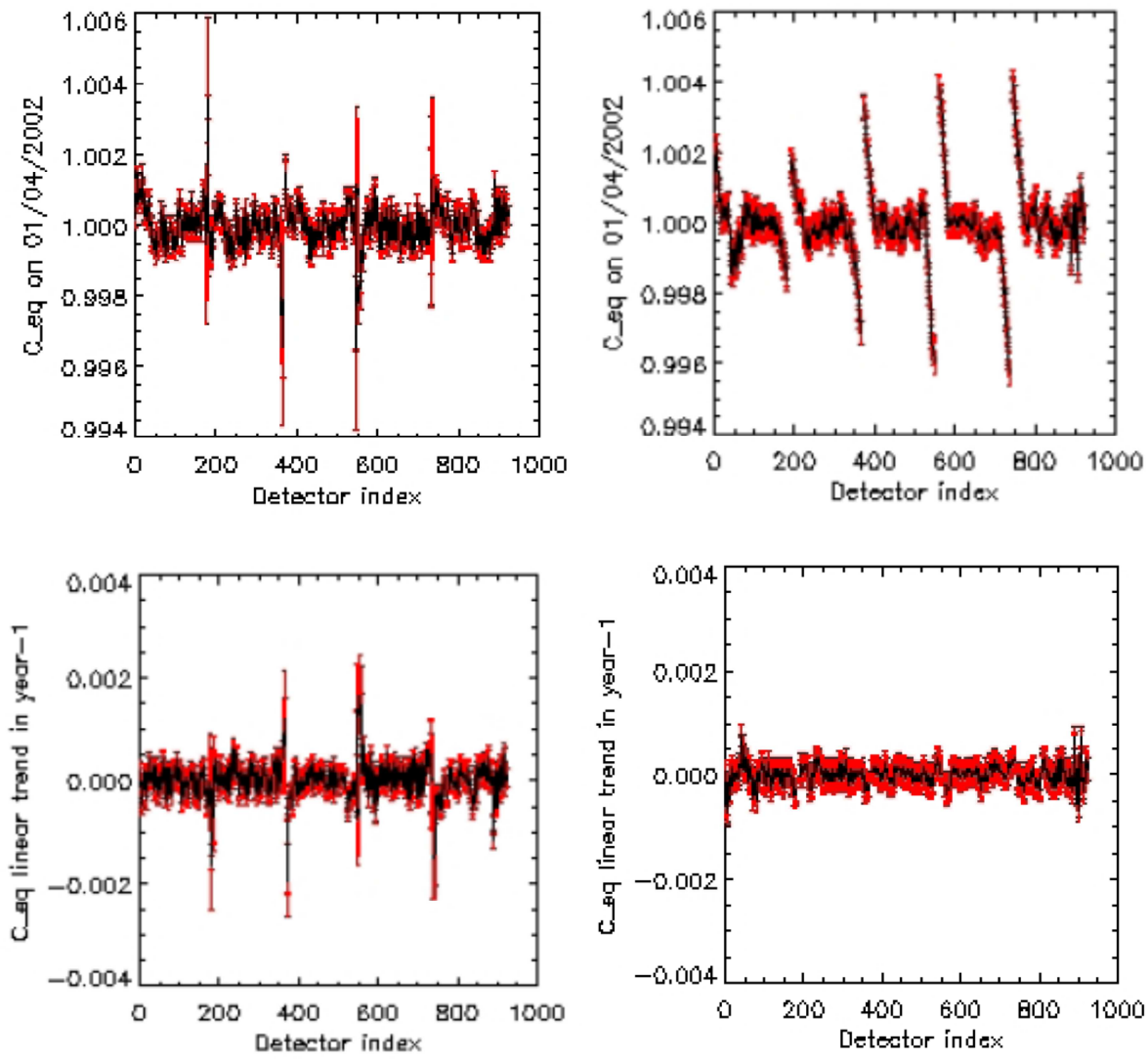

Figure 1: Comparison of (a) pixel to pixel variabilityat beginning of mission (top) and (b) calibration time stability (bottom) between 2nd (left) and 3rd (right) reprocessing Level 1b data over Antarctica.

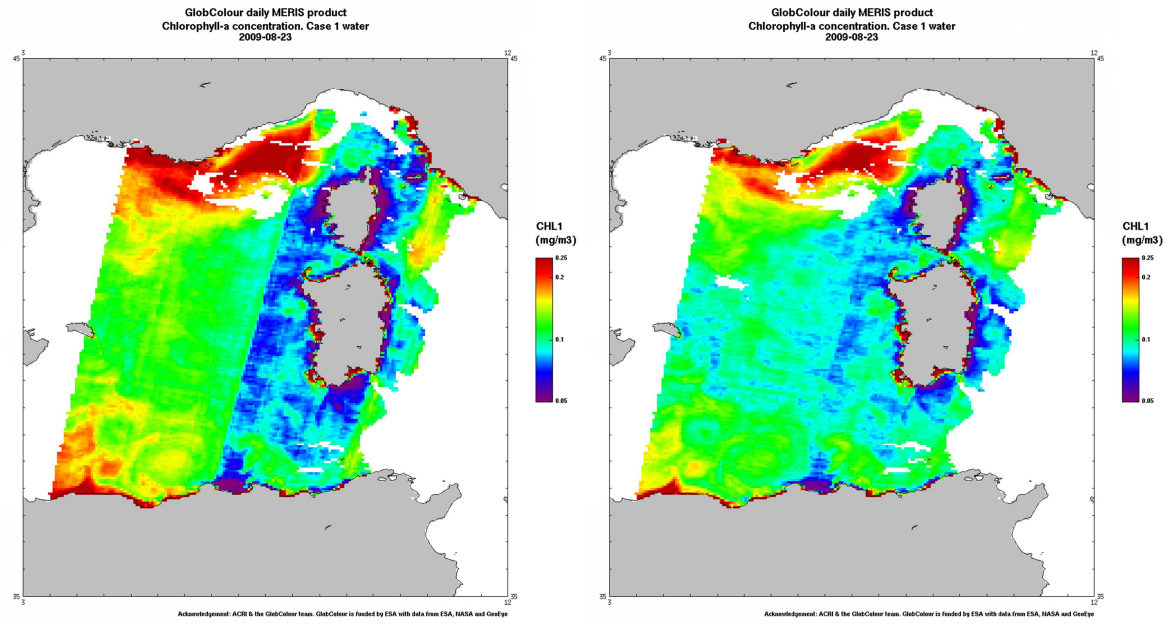

Product: CHL1

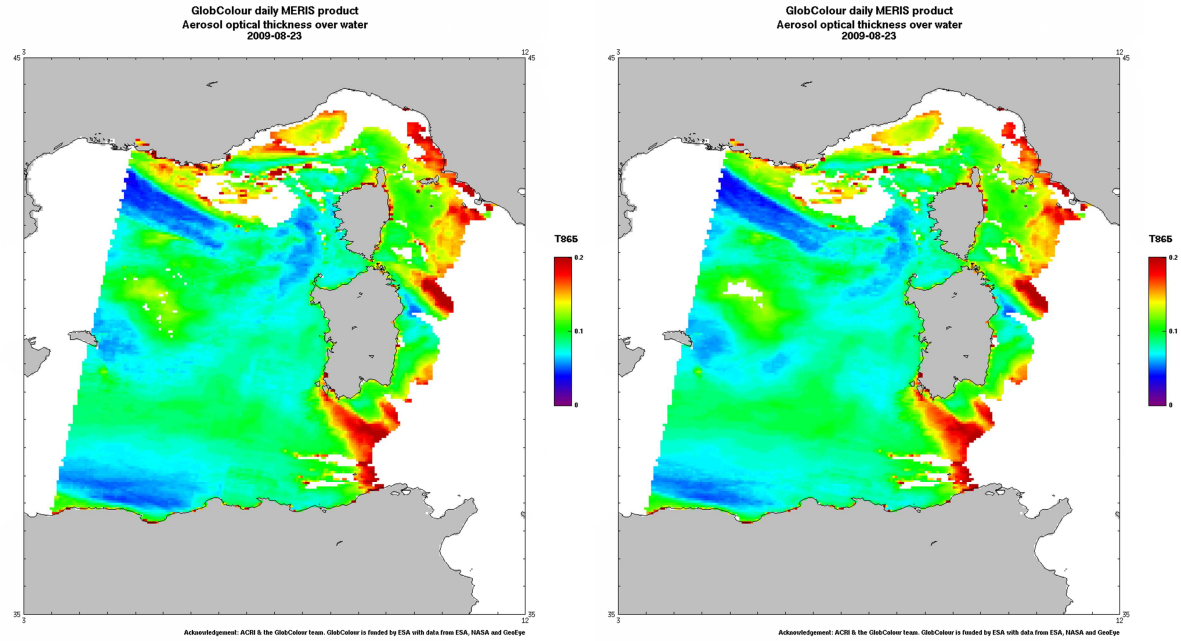

Product: T865

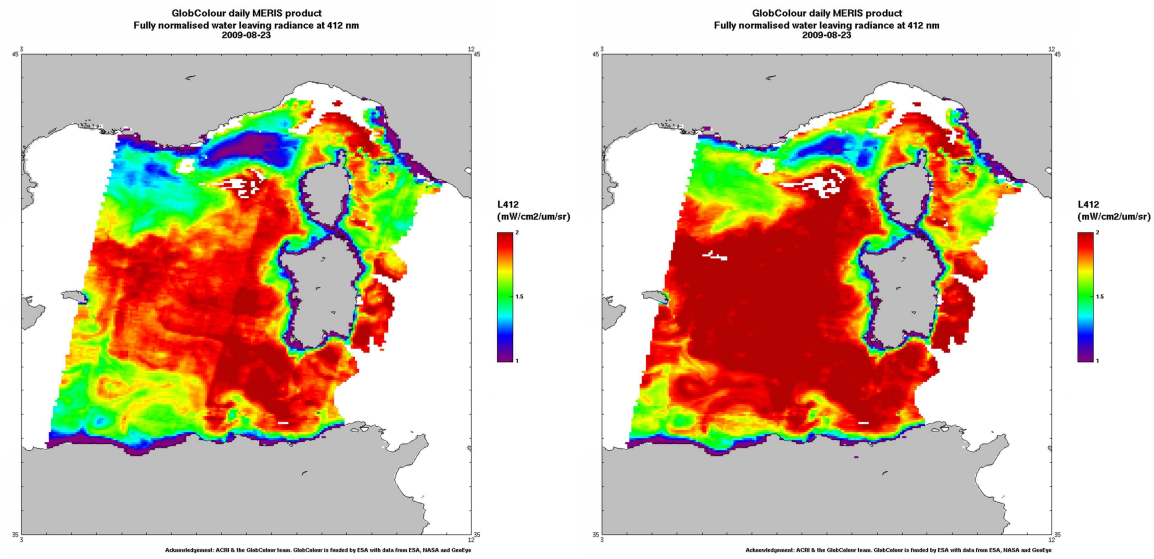

Product: L412

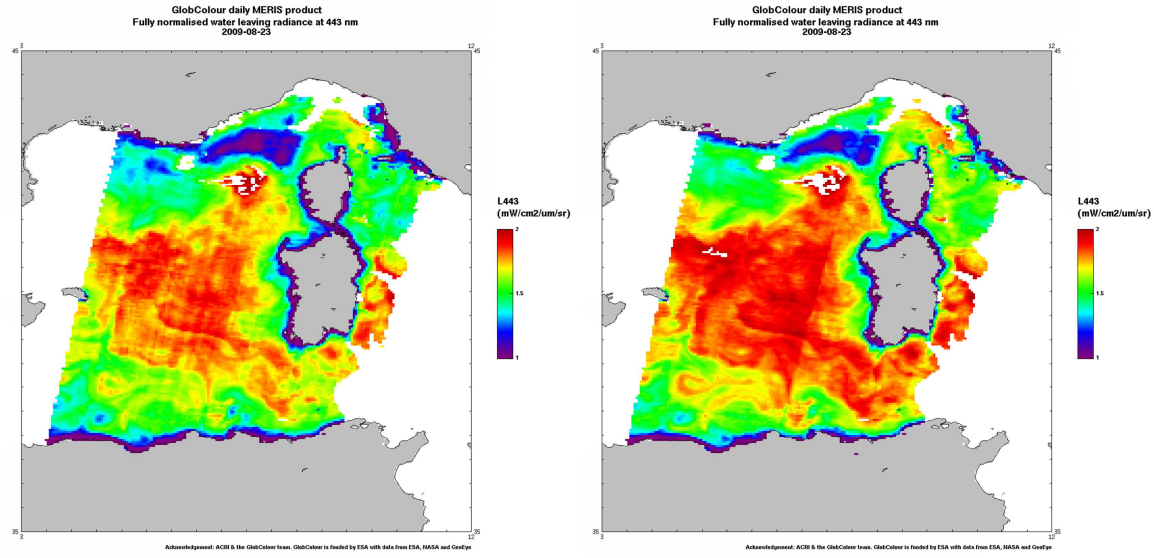

Product: L443

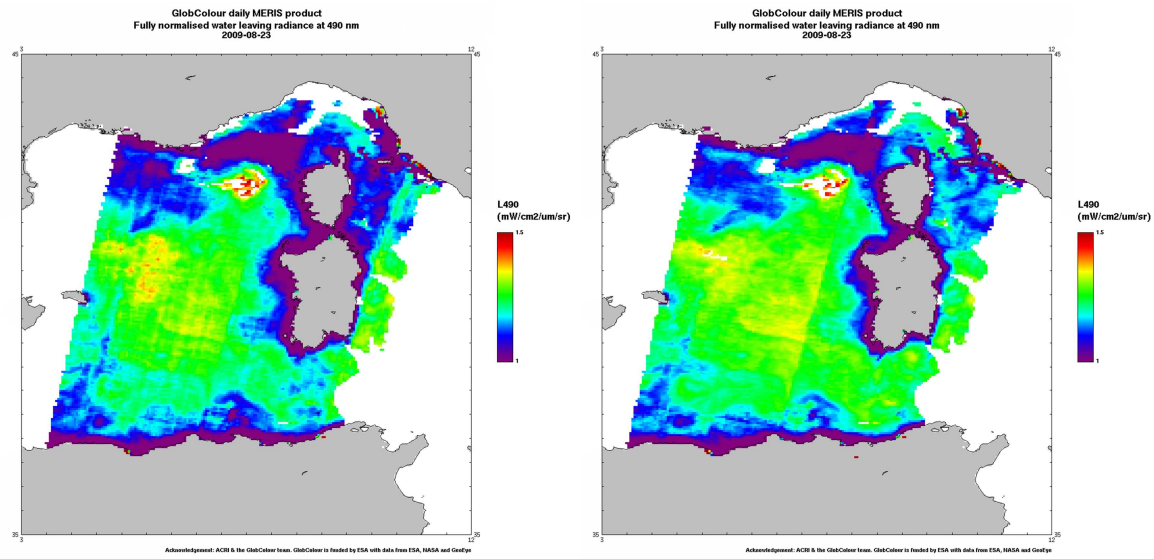

Product: L490

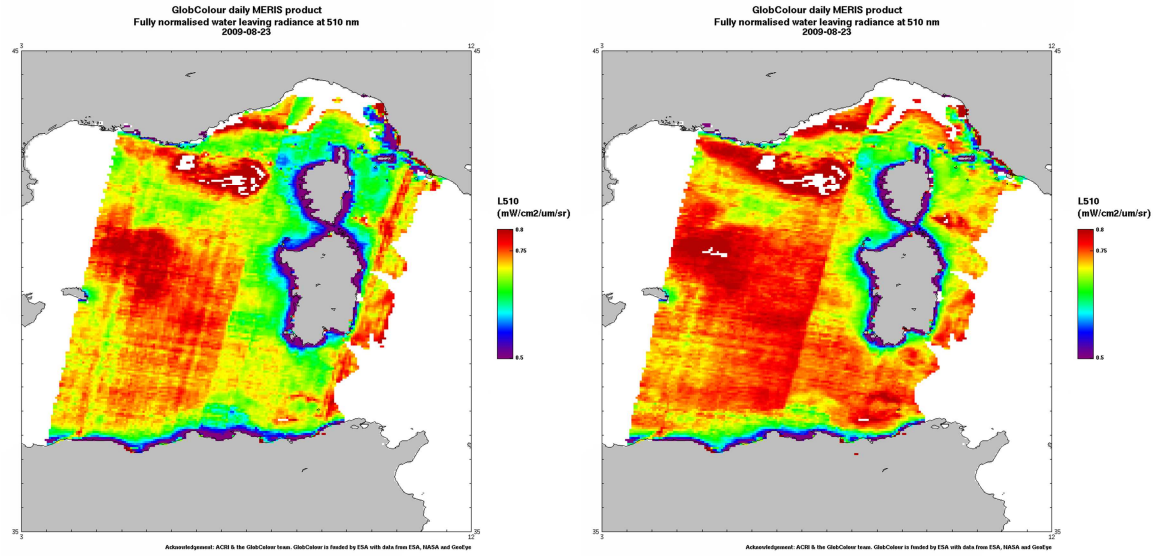

Product: L510

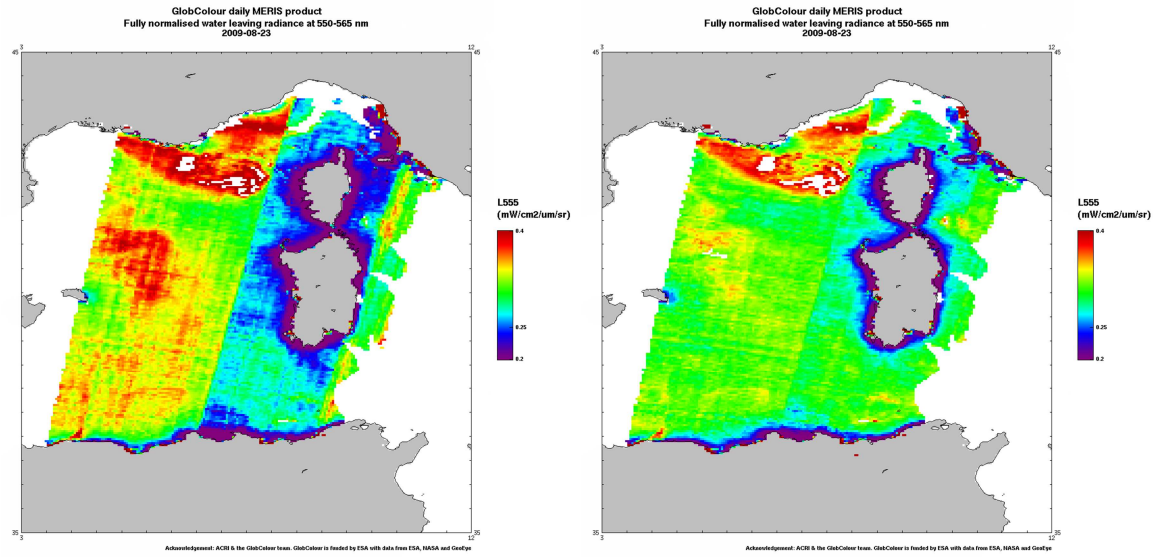

Product: L560

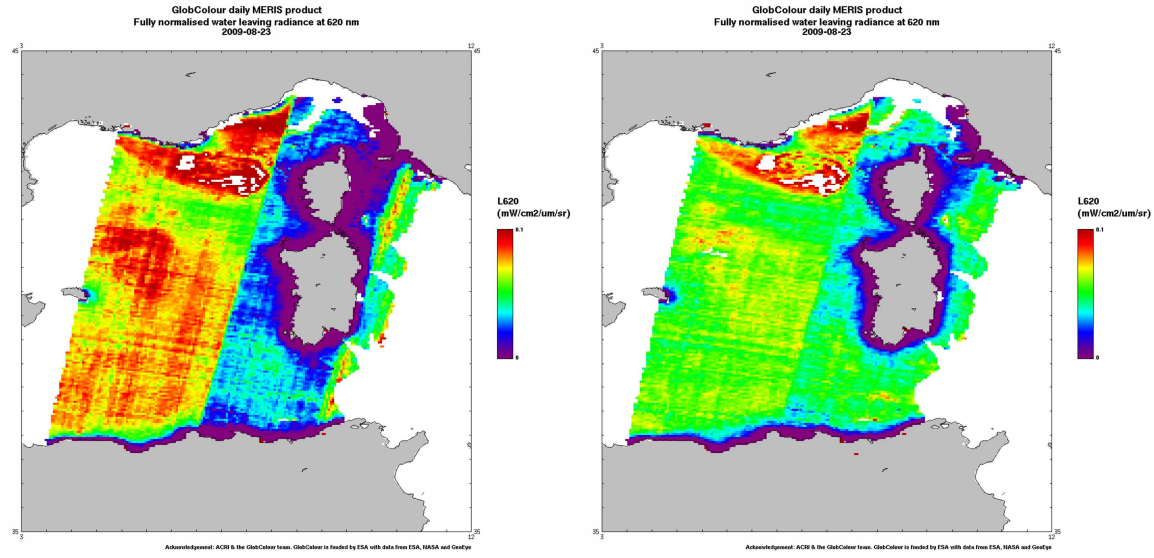

Product: L620

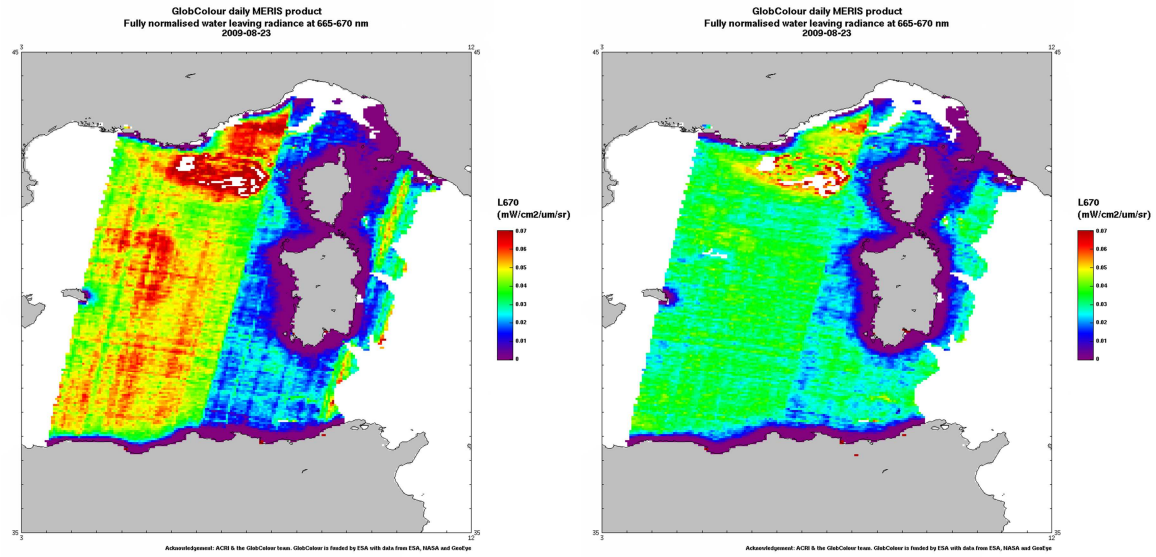

Product: L670

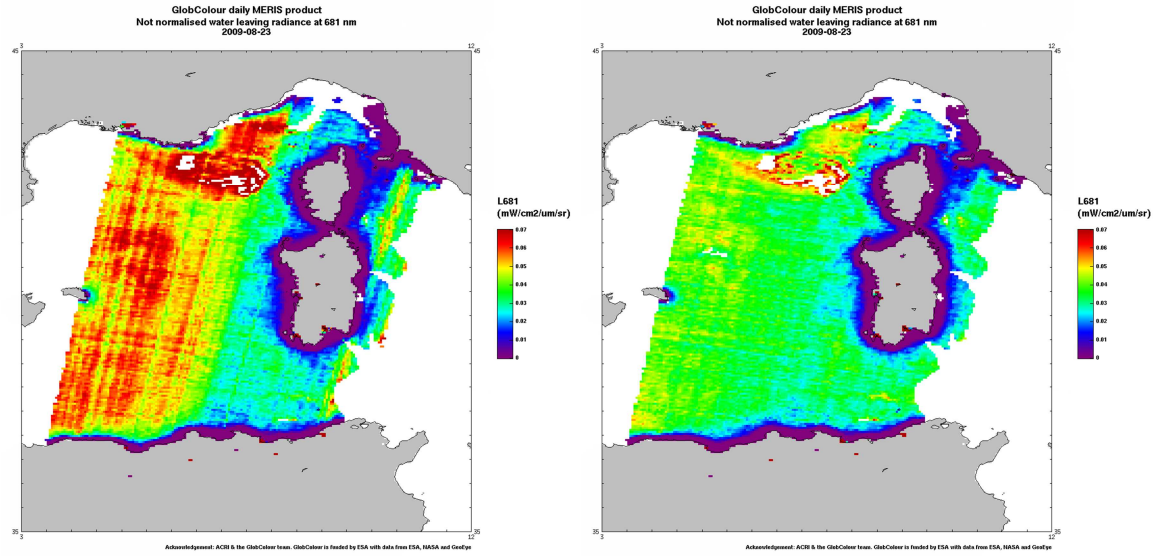

Product: L681

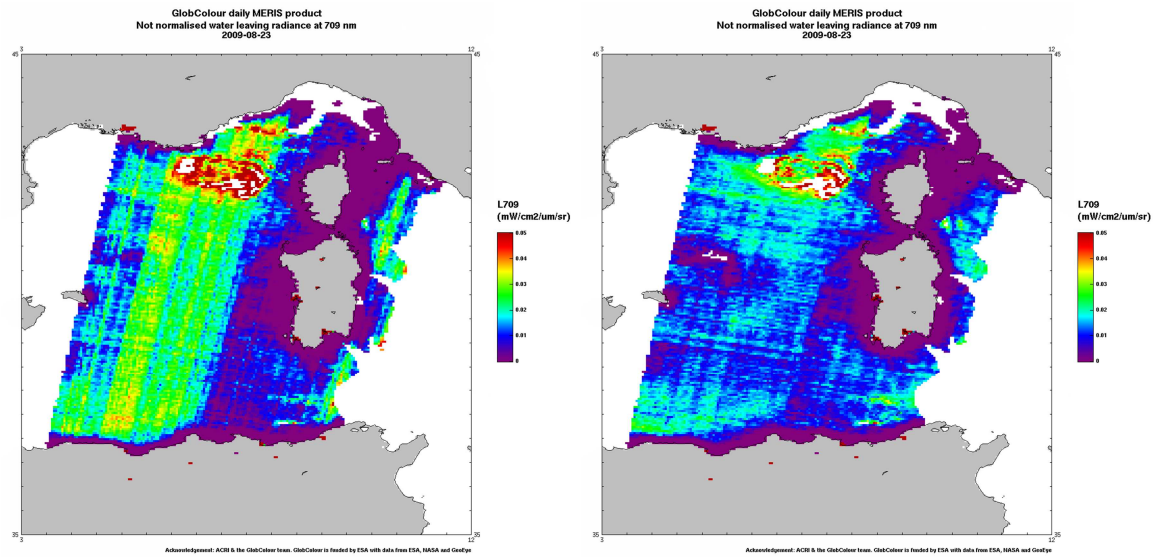

Product: L709

Figure 2: Effect of calibration on a Mediterranean scene (20090826) – Left: 2004 model, Right: 2009 model

References

MERIS Instrument Calibration, Bourg L. and S. Delwart, Proceedings of the MERIS Validation Team Meeting 2005 (download the PDF here).

MERIS Instrument Calibration, Status for 3rd re-processing, Bourg L. and S. Delwart, presentation to the MERIS Validation Team Meeting 2010.

3.2 Level 1 georeferencing

Contributor: Ludovic Bourg (ACRI-ST)

Purpose and description of changes

In order to allow a future evolution of the MERIS Level 1b processing and products toward ortho-geo-referencing, the nature of the instrument pointing auxiliary data has been updated to include full direction cosines at every pixel.

Ortho-geo-referencing shall be understood as per pixel parallax corrected three-dimensional geo-referencing accounting for Earth surface elevation, i.e. determination of the intersection of the line-of-sight of each pixel with the Earth surface represented by a Digital Elevation Model (DEM) on top of the WGS-84 reference ellipsoid. This is what is provided by the AMORGOS post-processing tool (http://earth.esa.int/object/index.cfm?fobjectid=4410). It is reminded that geo-referencing currently included in MERIS products is:

- Computed regardless of elevation, i.e. at the intersection between line-of-sight and the reference ellipsoid;
- Provided only on a sub-grid of the pixels (every about 16 km).

Impact, expected change on product

Slight geolocation differences can be observed.

4 Level 2 data processing – Common branch

4.1 Gaseous correction

Contributor: Jürgen Fischer (FUB)

4.1.1 Improvement of the O2 transmittance correction

Purpose and description of changes

Since the correction of oxygen absorption has been insufficient and led to errors in atmospheric correction, a more detailed correction procedure has been developed and integrated into O_2 corrections of the 3rd reprocessing.

The 778 nm MERIS band is located at the long-wave end of the oxygen A absorption band. Due to some isolated oxygen absorption lines, the transmission at 778 nm is slightly reduced as compared to a pure window channel. This offset is not constant but depends on the central wavelength of band 12 (spectral smile effect), the viewing geometry and the brightness of the observed scene [*Lindstrot, 2009*]. The effect of aerosol scattering is small for a given viewing geometry as the scattering appears in the lower atmosphere and there is hardly any effect on the average photon path length [*Lindstrot et al., 2009*].

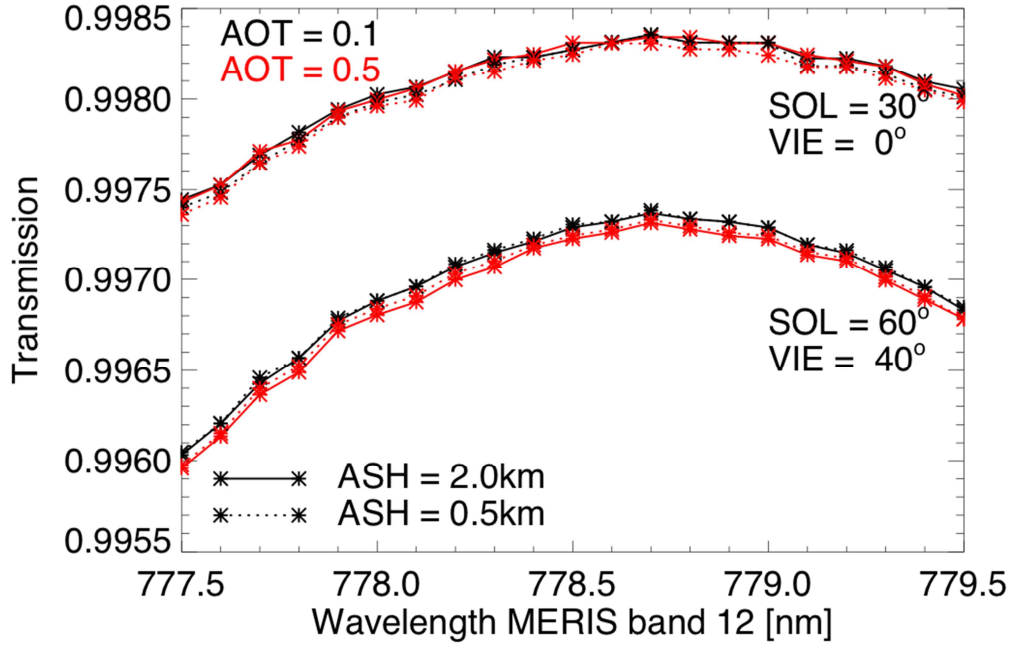

Figure 3: Transmission in MERIS band 12, depending on central wavelength for two viewing geometries, two aerosol loads (AOT) and two Aerosol Scale Heights (ASH).

Based on radiative transfer simulations performed with MOMO [*Fell and Fischer, 2001*], a 5 dimensional Look-Up Table (LUT), namely the central wavelength of band 12, the

normalized measured radiance of band 12, the solar and viewing zenith angles and the azimuth distance, has been created. In order to extract the transmission in band 12 from the LUT, a five-dimensional interpolation among the closest LUT grid-points has to be performed.

Impact, expected change on product

- Improvement of atmospheric correction and all procedures using MERIS band 12 at 779 nm.
- Less noise of the retrieved products is expected as well.

References

R. Lindstrot, 2009, Sensitivity study: Oxygen absorption in the 778nm band. ESA O2 Project (ref. ESRIN/AO/ 1-5161/07/I-OL), Technical Note.

R. Lindstrot, R. Preusker, J. Fischer, 2009, Description of the LUT-based correction of MERIS band 12. ESA O2 Project (ref. ESRIN/AO/1-5161/07/I-OL), Technical Note.

Fell, F. and J. Fischer, 2001 Numerical simulation of the light field in the atmosphere-ocean system using the matrix-operator method. J. Quant. Spectrosc. Radiat.Transfer, Vol.3, p.351-388.

4.1.2 Improvement of the H20 transmittance correction

Contributor: Francis Zagolski (Parbleu)

Purpose and description of changes

In the gaseous correction algorithm, the water vapour transmittances (T_{H2O}) in the slightly contaminated MERIS spectral bands (*i.e.*, bands number 4, 8, 9 10, 12, 13 & 14) are directly estimated with 3rd order polynomial fits expressed as function of the TOA radiances (L^*_{900}/L^*_{885}) between the 900 nm (strong absorption band) and 885 nm wavelengths [*Santer et al., 1999*]:

$$T_{H_2O}(\lambda,\vartheta_s,\vartheta_v,u_{H_2O},\rho_s,\tau^a)=\sum_{i=0}^{3}k_i(\lambda).\left(\frac{L^*_{900}(\vartheta_s,\vartheta_v,u_{H_2O},\rho_s,\tau^a)}{L^*_{885}(\vartheta_s,\vartheta_v,u_{H_2O},\rho_s,\tau^a)}\right)^i$$

where

- k_i are the polynomial coefficients;
- u_{H2O} is the total water vapour amount (g.cm^{-2});
- ρ_s is the surface reflectance;
- τ^a_ϵ is the aerosol optical thickness at 550 nm.

This approach accounts for the coupling between scattering and gaseous absorption.

These polynomial coefficients have been determined with simulations completed over a black surface with the RTC/GAME (Global Absorbing ModEl), using as input the coefficients of the exponential sum fitting technique (ESFT) generated separately by a Line-By-Line (LBL) code with the HITRAN2000 database for each of the MERIS spectral bands (*seeZagolski,*2011*(a, b)* for more details). Compared with the 2nd reprocessing, the molecular depolarization factor has been introduced in GAME.

Impact, expected change on product

Figure 4displays the new H2O transmittances in the 15 MERIS bands estimated with the polynomial fits that are used in the current 3rd reprocessing. Note that the strong absorption band at 900 nm has been discarded from this treatment ($T_{H2O}(900)$ being set to 1, here). Compared with the 2nd reprocessing, the introduction of the depolarization factor of molecules yields to relative differences less than 1% in absolute relative value whatever the ratio of TOA radiances (L^*_{900} / L^*_{885}) within [0.4; 0.9] (Figure 5).

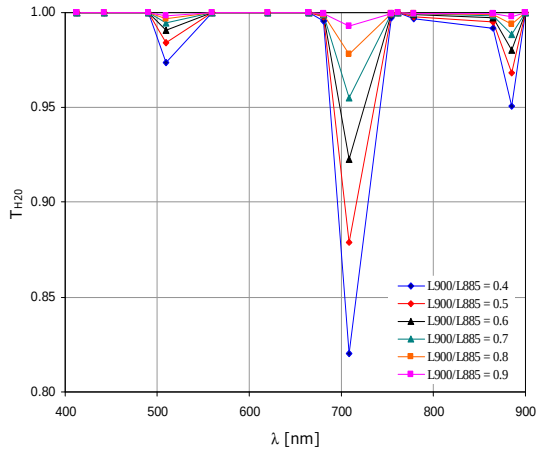

*Figure 4: H2O transmittances (TH2O) estimated with the 3rd order polynomial fits at the 15 MERIS wavelengths using a set of 6 values of (L*900/L*885)*

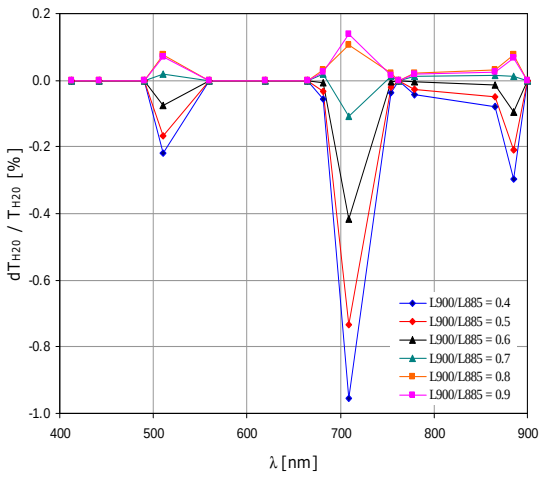

Figure 5: Relative differences in estimated TH2O between the 3rd and 2nd MERIS reprocessings

Consequently, this improvement should have to impact slightly on the MERIS TOA reflectances corrected for H_2O absorption, with a maximum bias of 1% in absolute relative value for the gaseous correction in band #9 (708.75nm) for the case of low values of the ratio (L^*_{900} / L^*_{885}).

References

Santer, R., V Carrère, P. Dubuisson, and J.C. Roger, 1999.Atmospheric corrections over land for MERIS, *International Journal of Remote Sensing*, 20 (9), pp. 1819-1840.

Zagolski, F, 2011*a*. Specification of the contents of the MERIS radiative transfer tools used to generate the level-2 auxiliary data products", *PARBLEU / ESA Report (PO-RS-PAR-GS-0002-3C): 'ENVISAT-1 Ground segment for MERIS'*, Quebec (Qc), Canada, Feb. 2011: 142p.

Zagolski, F, 2011*b*. Specification of the scientific contents of the MERIS level-1b & 2 auxiliary data products", *PARBLEU / ESA Report (PO-RS-PAR-GS-0002-3C): 'ENVISAT-1 Ground segment for MERIS'*, Quebec (Qc), Canada, Feb. 2011: 540p.

4.1.3 O3 transmittance

Contributor: Francis Zagolski (Parbleu)

Purpose and description of changes

MERIS data are corrected for the ozone absorption using pre-computed values of ozone optical thickness (τ^{O3}) in each of the 15 spectral bands. These calculations are completed with a LBL code using a spectroscopic database (HITRAN2000) and the MERIS filters [*Clough et al.*, 1992]. The ozone transmittance (T_{O3}) is then computed as:

$T_{O_3} = \exp[-M \cdot u_{O_3} \cdot \tau^{O_3}]$ where u_{O3} is the total ozone amount (cm-atm) and *M* the air mass.

For the 3rd reprocessing, the look-up table (LUT) of τ^{O3} has been refreshed using a better spectral integration on the MERIS filter compared with the previous generation for the 2nd reprocessing.

Impact, expected change on product

Figure 6 below gives the standard ozone optical thicknesses (τ^{O3}) and the associated transmissivities computed in the 15 MERIS spectral bands with the LBL (for the 2nd and 3rd reprocessings) and 6S codes. An accurate computation (LBL) stresses that slight absorptions appear in MERIS bands 1, 12, 13, 14 and 15. Outside this set of bands, 6S underestimates the O_3 optical thickness with a relative deviation lower than 10% in absorbing bands, but this does not have a great impact on the ozone transmittance. Consequently, compared to the 2nd reprocessing, this new set of O_3 optical thicknesses will have a negligible impact on the gaseous correction of TOA reflectances.

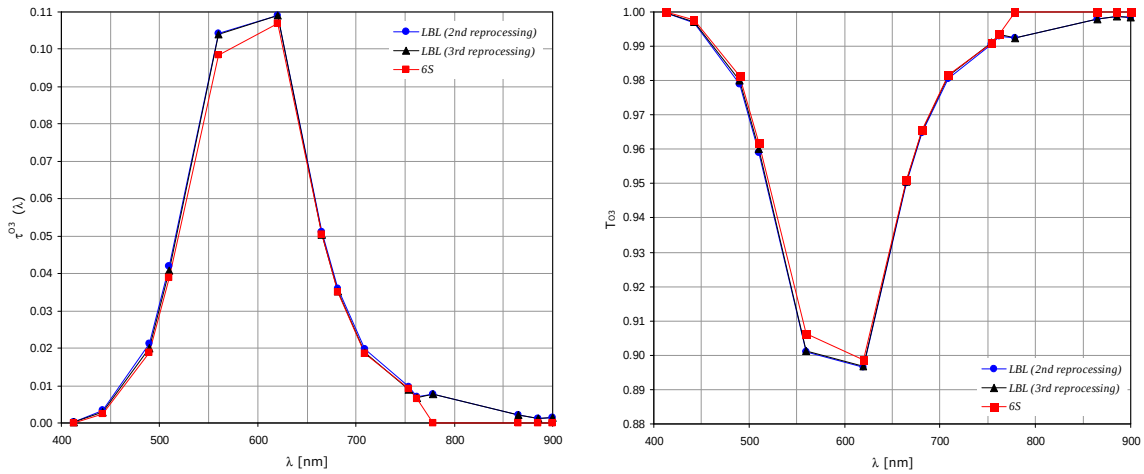

Figure 6: O3 optical thicknesses computed with the LBL code in the 15 MERIS filters (left) and corresponding O3 transmittances computed for an air mass of 1 and a total ozone amount of 1 cm-atm (right). Results are displayed for the 2nd and 3rd reprocessings and the 6S computations are depicted for a simple comparison.

References

Clough, S.A., M.J. Iacono, and J.L. Moncet, 1992. "Line-by-line calculations of atmospheric fluxes and cooling rates: Application to water vapor", *Journal of Geophysical Research*: 97, pp. 15761-15785

4.2 Pixel classification

Contributors: Carsten Brockmann (Brockmann Consult) and Ludovic Bourg (ACRI-ST)

The primary objective of the pixel classification is to identify the surface type of the pixel as being ocean, land or cloud, in order to submit it to the corresponding subsequent processing branch.

The secondary objective is to assign certain classification flags, called science flags, which described further characteristics of the pixel. These are, for example, sun glint over water or snow/ice on land and water surfaces.

The pixel classification has been significantly revised for the 3rd reprocessing. The main changes are:

- Addition of information on the height of the scattering surface in the cloud detection (derived from the O2 band measurement),
- Addition of an identification of snow/ice.
- Addition of numerous other improvements, all being described in the following sections.
- It should also be mentioned that the implementation of the pixel classification logic has been changed from 2nd to 3rd reprocessing, from a table driven approach to coding directly the logical combinations. This improves transparency and maintainability of the code.

4.2.1 Identification of Cloud pixel over water

Purpose and description of changes

Summary

In 2nd reprocessing, too few clouds were detected over water; only optically thick and bright clouds were detected. Many pixels at cloud borders, less bright scattered clouds and thin clouds such as cirrus clouds were not identified. Most of these pixels lead to failure of one of the subsequent processing steps and the Product Confidence Data (PCD) was raised. However, still a significant number of undetected cloud pixels passed all processing steps and resulted in errors in water products retrieval. On the other hand, all undetected cloud pixels missed the cloud processing branch and the statistical quantities derived for clouds were degraded.

In the 3rd reprocessing, additional tests have been introduced that lead to identification of more clouds. In summary, there are now three kind of tests applied in order to identify cloudy pixels: two bright tests and one pressure test. These cloud tests are followed by a test on snow/ice in order to recover these pixels (they should not go to the cloud processing

branch, but will also not provide valid water products. They are flagged as ice_haze and PCDs are raised for all L2 products).

First bright test

In 2nd reprocessing, the cloud detection over water was performed with a single test that compared the reflectance in the blue with a threshold. This test is maintained in 3rd reprocessing and is called now the first bright test. Specifically, this test compares the Rayleigh corrected reflectance with a theoretically maximum expected reflectance, assuming a water with large amount of sediment – leading to strong scattering – and a turbid atmosphere with maritime aerosol. This threshold depends on sun and viewing geometry and is tabulated in a look-up-table (LUT).

Second bright test

In the 3rd reprocessing, this first bright test is complemented with a second bright test that compares the Rayleigh corrected reflectance in the blue with a global constant threshold. This threshold is generally lower than the LUT and thus, flags pixels particularly at the borders of clouds and less bright, scattered clouds. However, this second bright test cannot be applied where the underlying surface can be bright without being a cloud. One condition when this can happen is high sun glint, and consequently the second bright test is not applied when the high sun glint flag is activated. The second condition is the coastal zone. The MERIS L1b coastline flag is geometrically not very accurate and can be misplaced slightly. In tidal areas the actual water – land separation is anyway time dependent. Thus, it can happen that the cloud screening over water is applied to non-water pixels, and unfortunately (from the point of view of cloud detection) bright sandy beaches are quite common in the coastal zone. Therefore the second bright test is not applied in a buffer of 1 pixel around the coastline.

Pressure test

Optically thin clouds are not detected by either of the bright cloud tests. Such clouds are typically cirrus clouds and contrails. They impact severely the quality of the retrieval of water products. Such optically thin clouds can be detected by estimating the height from which the radiation is scattered. This information can be gathered from the measurement in the oxygen absorption band (O2 A-band). The measured signal is an integral mixture of photons that passed the cloud and which are reflected from the earth surface, and photons which are reflected by the cloud. The O2 A signal can be related to height of the scattering surface. While this is discrete and real quantity when the scattering surface is the earth surface for clear sky conditions, and the cloud top pressure for totally cloudy conditions, it is an apparent height of the mean scattering surface in the above described case of semi-transparent clouds. The algorithm for the retrieval of the apparent pressure estimation over water is described in *Santer & Aznay (2008)*. This apparent height is lower than the real height of the cirrus cloud but also higher than the earth surface. Over water, this quantity can be estimated rather well; the water surface can be assumed as black and being at 0 altitude, which reduces the uncertainty in the retrieval of the apparent scattering height. A

global threshold can be applied in order to decide that many photons are scattered from an altitude above sea level and thus indicating a thin cloud.

Because of the inaccuracy of the coastline as discussed above, the pressure test is also not applicable in the vicinity of the coastline and is disabled there.

Impact, expected change on product

There are two major changes compared to the 2nd reprocessing.

- Outside sea ice, more pixels are now classified as cloud than before. The borders of clouds, spatially scattered clouds, mixed pixels with a substantial amount of cloud contribution and optically thin clouds are now identified as clouds. In 2nd reprocessing most of these pixels could not be processed correctly to water products and the PCD_1_13 (atmospheric correction) and/or PCD_15 (Case_1 products) and/or PCD_16/17 were raised;
- Sea ice now gets the pixel type water, but is flagged as ice_haze, *i.e*. these pixels go to the water branch instead of the cloud branch. This is further discussed below.

Looking at a product without sea ice as a whole, this has the following impact

- The number of water pixels is decreased;
- The number of cloud pixels in increased;
- The number of PCD flagged water pixels is decreased: Most of the changes fall into this category because most previously undetected clouds were PCD flagged;
- The number of obviously wrong, but not PCD flagged, water products are decreased: this concerns only a smaller part of the pixels because previously most undetected clouds were PCD flagged;
- Average values of water products become more accurate.

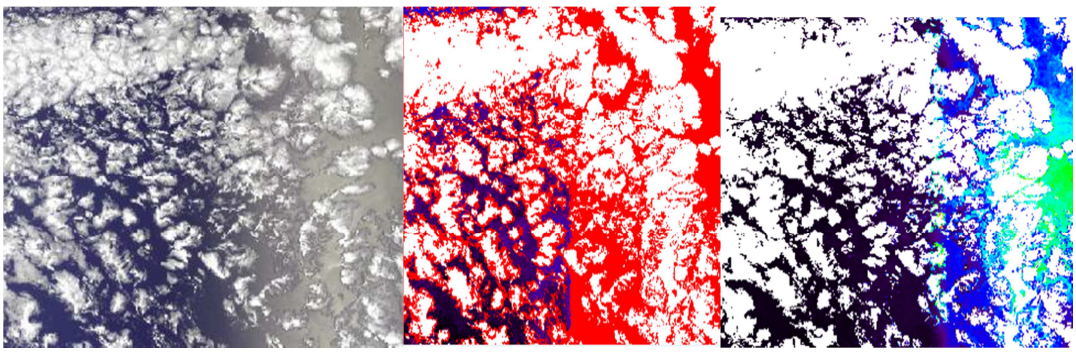

Figure 7: Example of the new cloud screening over the ocean. MERIS scene of 23.12.2008. Left: RGB, centre: 2nd reprocessing classification; right: 3rd reprocessing. White = cloud, red=PCD flagged. The values in the background of the centre and right image are the algal2 product.

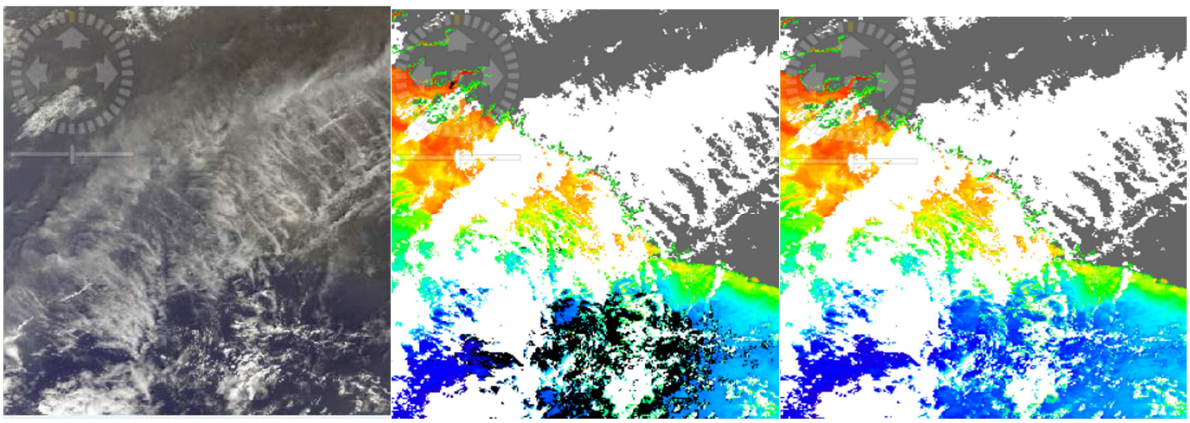

Figure 8: Example of the new cloud screening over the ocean, at the example of the algal_2 product. MERIS 19.12.2008 Ivory Coast. Left: RGB, centre: algal_2 with clouds (white) and PCD_16 (black). Right: agal_2 with clouds (white) and PCD_16 (black).

References

R. Santer, O. Aznay, 2008: The O2 apparant pressures over the ocean, ATBD. Report from the ESA O2 Project. Available on http://www.brockmann-consult.de/cms/web/beam/forum/-/message_boards/message/52322

4.2.2 Identification of Cloud pixel over Land

Purpose and description of changes

The cloud screening over land suffered from insufficient detection of clouds; many less bright or optically thin clouds were not detected. The cloud screening of the 2nd reprocessing relied fully on a single test on reflectance in the blue, with subsequent recovery of bright land, snow and ice tests using spectral slope tests. The bright test compared the Rayleigh corrected reflectance with a maximum reflectance of a vegetated land surface and a turbid atmosphere. This threshold depends on sun and viewing geometry and is stored in a look-up-table. Non vegetated bright surfaces (e.g. sand, snow) are flagged by this bright test and are restored as land using spectral slope tests in the VIS and NIR.

The bright test is kept for the 3rd reprocessing. However it was found that the slope tests are not working properly and they are no longer applied. Instead, a dedicated ice/snow test is applied (see section 7.5).

A bright test does not capture optically thin clouds, less bright clouds and spatially mixed cloud/land pixels. These pixels are now identified by a newly introduced test on the apparent height of the scattering surface. The principle of this test has been described above (section 4.2.1). However, over land surface the assumption of a black surface is not true and the contribution from Rayleigh and multiple scattering cannot be estimated with the same accuracy as over water. Only a rougher estimate of the apparent height of the scattering surface is possible. Further, the elevation of the terrain needs to be taken into account. The algorithm for the retrieval of the apparent pressure estimation over land is described in *Santer & Aznay (2008)*. The test compares the apparent height of the scattering surface with

the surface elevation. If the difference exceeds a certain threshold it can be assumed that a cloud is present in the pixel.

Impact, expected change on product

The introduction of the pressure test leads to the identification of additional pixels as clouds. This reduced the number of PCD flagged pixels and the statistical values (spatial and temporal averages, variances, Level 3 products) of the land products. Visual artefacts due to residual clouds will be reduced.

However, while working with the new pressure test it was found that the difference between the elevation of the surface and the apparent height of the scattering can be influenced strongly by the atmospheric conditions of the scene. While in very many cases a difference (the height being expressed in pressure for this test) of ~150 hPa is sufficient to reliably differentiate between surface and cloud, there are a few cases, mostly with a foggy atmosphere, when this value is not working and when it leads to unacceptable results. This is a bad situation for an operational and global algorithm; the threshold has to be driven by the worst case, and thus the threshold has to be increased to 250 hPa. As a consequence, in many products thin clouds are still not detected although it would be possible using the pressure test. The work will be continued to improve either the estimation of the apparent pressure value or to find a method to adapt the threshold to the atmospheric conditions.

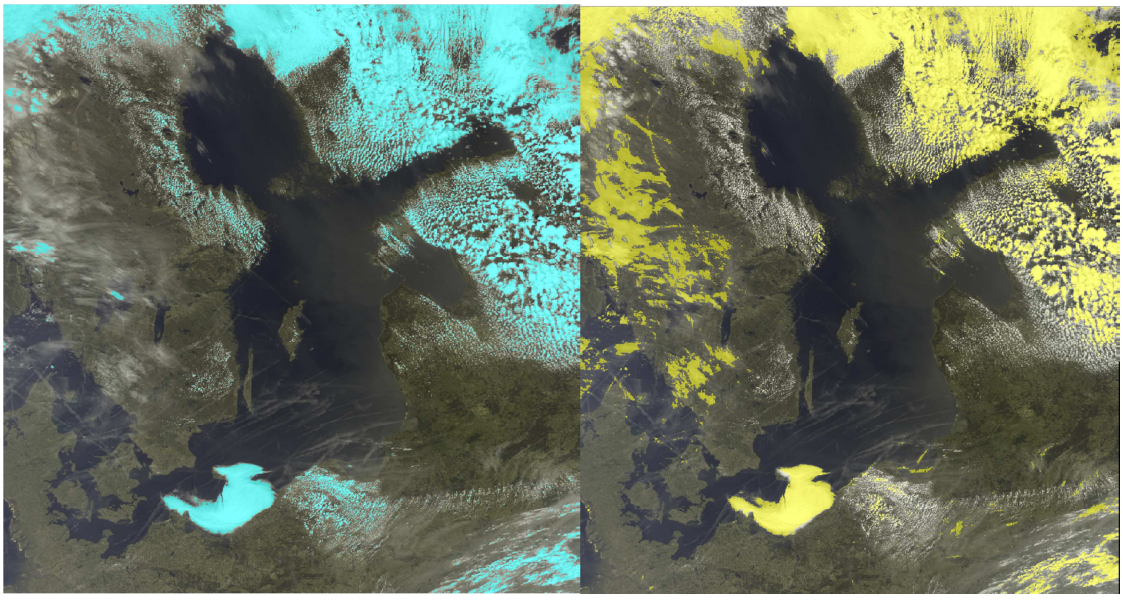

Figure 9: MERIS 01.06.2003 with cloud screening over land. Left: 2nd reprocessing, Right: 3rd reprocessing.

References

R. Santer, O. Aznay, 2008: The O2 apparant pressures over the ocean, ATBD. Report from the ESA O2 Project. Available on http://www.brockmann-consult.de/cms/web/beam/forum/-/message_boards/message/52322

4.2.3 Identification of Snow/ice pixel

Purpose and description of changes

In the 2nd reprocessing, the identification of snow and ice was not well developed. Over land, a restoration test was applied to pixels which are identified as bright by a bright test, but the purpose of this test was not to positively detect snow and ice, but to reduce misclassification of cloud pixels (Note this is consistent with the MERIS L2 processing and products, where no snow processing is foreseen, but a dedicated cloud branch exists). This restoration test did not work very efficiently and most snow and ice pixels were classified as clouds.

While both, clouds and snow are very bright in the visible and near infrared, snow absorbs strongly in the SWIR spectral region. This is exploited by commonly used differential snow index tests. Unfortunately MERIS does not have a SWIR band. In the framework of the ESA SnowRadiance project (http://wfaa-dat.esrin.esa.int/stse/projects/summaryp103.asp), it was found that the increase of absorption is already notable in MERIS longest NIR band 14 (885 nm), and that the slope between bands 13 (865 nm) and 14 can be used for a reasonable approximation of a normalized differential snow index. This has been called the MERIS Differential Snow Index (MDSI) where MDSI = (toa_ref_13 – toa_ref_14) / (toa_ref_13 + toa_ref_14). The algorithm is described in *Brockmann and Krüger (2010)*.

A test has been introduced where the MDSI is compared with a global threshold. This test is applied only to pixels which have been classified as bright beforehand (which are different tests over land and water).

Pixels which have been identified as snow/ice get the surface type of the underlying surface (land or water, according to the L1b flag). Over water, the positive MDSI test triggers the ice_haze flag (see § 6.8). Over land, it is written as a new flag into the product (see § 7.5).

Impact, expected change on product

In 2nd reprocessing snow and ice pixels were very often classified as clouds; due to their spectral similarity with clouds the cloud algorithms delivered very often a “valid” cloud product, i.e. the cloud PCD were not raised. This strongly affected the quality of statistical quantities of cloud products (averages, variances, frequency of occurrence) and the cloud Level 3 products.

In 3rd reprocessing the separation between snow/ice and clouds works reasonably well; the number of misclassified cloud pixels is significantly reduced leading to much better statistical values and Level 3 products.

The visual appearance of cloud products over snow areas has improved substantially due to this change.

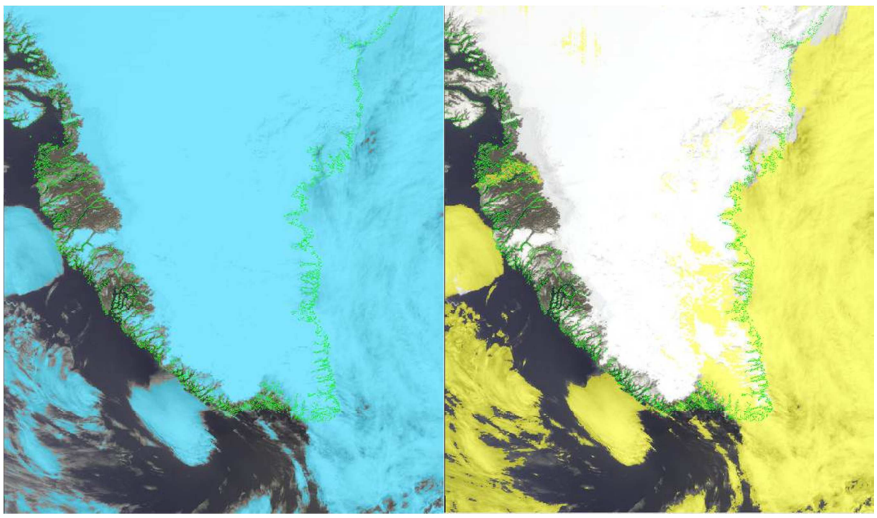

Figure 10: MERIS 05.06.2003, Greenland. Left: 2nd reprocessing, cloud mask in blue. Right: 3rd reprocessing, clouds mask in yellow. These figures are an enlargement of the product shown in Figure 11 below.

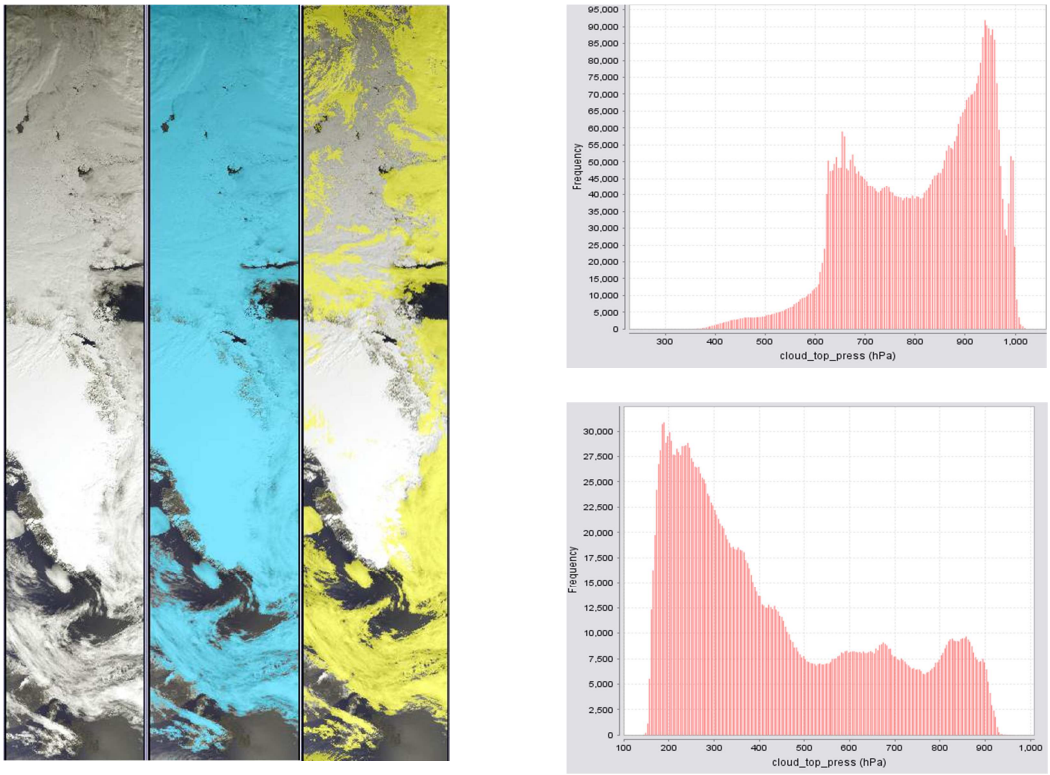

Figure 11: Impact of snow identification on histogram of CTP(MERIS 05.06.2003, Greenland. Left three images: first: RGB, second: 2nd reprocessing classification (cloud= blue), third: 3rd reprocessing (cloud=yellow). Right figures: Corresponding histograms of CTP of cloud pixels.Top: 2nd reprocessing; the peak of the CTP histogram is at 960 hPa and the average value at 809 hPa. The histogram shows the disturbing effect of snow pixels being classified as clouds and leading to very high pressure values. Bottom: 3rd reprocessing; peak at 250hPa and mean values at 433 hPa.

References

Brockmann, C., Krüger, O. (2010) Snow Radiance Cloud Snow Ice Identification ATBD. Available on http://www.brockmann-consult.de/cms/web/beam/forum/-/message_boards/message/52330

5 Level 2 data processing – Cloud branch

5.1 Cloud Top Pressure

Contributor: Jürgen Fischer (FUB)

Purpose and description of changes

The past 2nd MERIS data reprocessing used to derive prominent camera boundaries along the MERIS swath with cloud top pressure jumps up to 50 hPa. In the case of MERIS measurements in the O_2 A-band, one of the largest sources of error is instrumental stray light [*Lindstrot et al. 2009*]. An empirical stray light correction has been derived from a new surface pressure algorithm, a digital height model and the use of ECMWF surface pressure values [*Lindstrot et al., 2010*]. The surface albedo, derived now from MERIS data, is introduced with a spatial resolution of 0.05° by 0.05°. The previous surface albedo was taken from GOME with a spatial resolution of 1° by 1°.

The cloud top pressure algorithm, based on a neural net approach, has not been changed. Only the input data have been improved, leading to a more accurate and consistent cloud top pressure product.

Impact, expected change on product

Significant reduction of camera boundary jumps and a more accurate cloud top pressure along the full MERIS swath is expected. Together with a more detail and accurate surface albedo the cloud top pressure product is more consistent and accurate in the 3rdreprocessing.

References

Lindstrot, R., R. Preusker, and J. Fischer, 2009, The retrieval of land surface pressure from MERIS measurements in the oxygen A band, J. Atmos. Oceanic Technol., Vol.26, p.1367–1377.

Lindstrot, R, Preusker, R. and Fischer, J., 2009, Remote Sensing of Multilayer Cloud-Top Pressure Using Combined Measurements of MERIS and AATSR Onboard ENVISAT, J. Appl. Meteor. Climatol., Vol.49, p.1191-1204.

Lindstrot, R., R. Preusker, and J. Fischer, 2010, Empirical Correction of Stray Light within the MERIS Oxygen A-Band Channel, Atmos. Oceanic Technol., Vol.27, p.1185–1194.

6 Level 2 data processing – Ocean branch

6.1 Smile correction

Contributor: Jean-Paul Huot (ESA)

Purpose and description of changes

Smile correction is a simple method aiming at reducing variability introduced in Level 2 products by the in-FOV variation of the channels central wavelengths: the so-called MERIS smile effect. This effect and current correction methodology are described in details in a technical note [*Bourg et al*, 2008]. Let us just recall here the two steps correction:

1. Radiance to reflectance conversion takes smile effect into account through the use of per pixel in-band equivalent irradiance,
2. TOA reflectance is corrected for in-FOV wavelength variations by linear interpolation.

The implemented improvement of the second step is limited to clear sky water pixels and takes advantage of the well-known spectral shape of the molecular scattering contribution to the TOA signal to improve correction accuracy. The reflectance correction is now split into three steps:

1. Estimate Rayleigh reflectance at pixels wavelength by log-linear interpolation of the LUT for the current pixel. The rationale behind that is that Rayleigh reflectance closely follows a power law and thus log-linear interpolation is much more accurate than linear;
2. Obtain Rayleigh corrected reflectance at pixel's wavelength, by subtracting result of item 1, and correct it for smile by the usual linear interpolation scheme;
3. Go back to TOA by adding Rayleigh reflectance at nominal wavelength to the smile-corrected Rayleigh corrected reflectance.

Impact, expected change on product

Expected impact on TOA reflectance is very small, as smile effect is already relatively small (few tenths of a percent), but overall accuracy should be improved and sensitivity to radiometric noise should be reduced.

References

Bourg, L., L. D'Alba, P. Colagrande, 2008,MERIS Smile Effect Characterization and Correction, ESA technical Note,available at http://earth.eo.esa.int/pcs/envisat/meris/documentation/MERIS_Smile_Effect.pdf

Delwart, S., R. Preusker, L. Bourg, R. Santer, D. Ramon and J. Fischer, 2005. MERIS in-flight spectral calibration, International Journal of Remote Sensing, MERIS Special Issue, Volume 28, Numbers 3 - 4, January 2007

Delwart, S., R. Preusker, L. Bourg, R. Santer, D. Ramon & J. Fischer, MERIS In-flight Spectral Calibration, Proceedings of the Second working meeting on MERIS and AATSR Calibration and Geophysical Validation, "MAVT-2006", available at http://envisat.esa.int/workshops/mavt_2006/papers/60_delwa.pdf

6.2 Vicarious adjustment

Contributors: Constant Mazeran (ACRI-ST), Christophe Lerebourg (ACRI-ST), Jean-Paul Huot (ESA-ESTEC) and David Antoine (LOV)

Purpose and description of changes

The MERIS 2nd reprocessing used to overestimate water leaving reflectance up to 20% at shorter wavelength, as assessed by match-up comparisons with *in-situ* measurements (see e.g. [*Antoine et al 2008*], [*Zibordi et al 2006]*, [*MERMAID*] and plots hereafter*)*. It is agreed that Level 1 calibration alone is not able to correct this bias and to reach requirement of 5% error uncertainties. A vicarious calibration is therefore required and has been implemented for the first time in the MERIS 3rd processing.

The principle consists in directly multiplying the TOA reflectances by corrective gain factors g(λ), for each wavelength λ, in such a way to remove bias in marine reflectance after atmospheric correction [*Franz et al 2007*] [*Bailey et al 2008*]. The set of gains is assumed to be unique for all observation geometries and throughout the whole mission. Determination of gains relies on comparison between actual and *targeted* reflectances on a reference dataset, mainly build upon *in situ* measurements.

In the case of MERIS, whose wavelengths are detector dependent, decision has been made to apply the correction at Level 2, after the sequential corrections for gaseous absorption, stratospheric aerosols, smile effect and glint correction, i.e. on the so-called ρ_{gc} reflectance:

$$\rho_{gc}^{vic}(\lambda) = g(\lambda)\rho_{gc}(\lambda)$$

This explains the denomination of an *adjustment* (rather than a calibration), which corrects for both potential instrumental and algorithmic source of error, in particular in the atmospheric correction whose input is ρ_{gc}.

Details on the exact gain computation, methodology, datasets and sensitivity analysis can be found in [*Lerebourg et al 2011*]; they can be schematically summarised in two steps:

1. A first adjustment of the 865 nm band whose purpose is to align it on a theoretical spectral shape followed by the other NIR bands (power law for aerosol reflectance). This computation is conducted on oligotrophic region where the marine signal in the NIR is approximated by pure sea water reflectance.
2. The vicarious adjustment itself of the visible bands, based on *in situ* measurements from MOBY and BOUSSOLE mooring sites.

Vicarious gains and associated dispersions are plotted on Figure 12. A new field containing the values has been added to the Ocean Aerosol Auxiliary Data File and can be modified in ODESA.

Impact, expected change on product

In view of an operational processing, the approach is mainly justified on the open ocean. In the blue bands, gains lower than the unity mechanically tend to decrease the marine reflectance and remove most of the bias observed in previous reprocessing (Figure 13). On more than 300 MOBY and BOUSSOLE matchups, it yields to relative percentage difference lower than 5% for all bands between 412 and 560 nm. Note that the validation dataset is not identical to the one used for gain computation.

The NIR adjustment itself has a positive impact on clear waters (not shown here) whereas it may produce artefact in turbid waters (negative reflectances) because of interaction with the Bright Pixel Atmospheric Correction (BPAC). It is worth noting that alternative implementations of the BPAC are much less sensitive to the NIR adjustment and do not degrade number of valid pixels. Hence the vicarious adjustment in coastal waters is tributary of other issues and should be considered with caution.

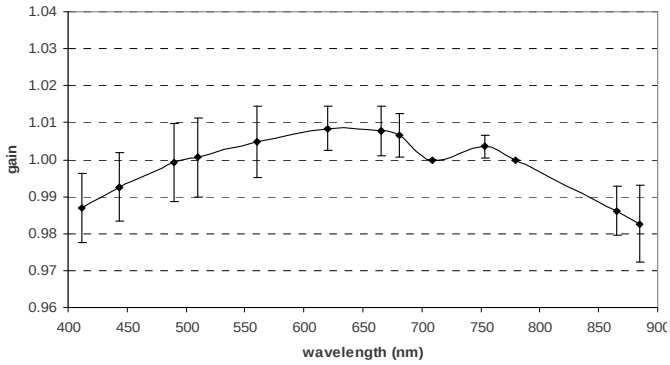

Figure 12: Gain spectrum and related standard deviation implemented in MERIS 3rd reprocessing

References

Antoine, D., F. D'Ortenzio, S. B. Hooker, G Bécu, B. Gentili, D. Tailliez, and A. J. Scott (2008), Assessment of uncertainty in the ocean reflectance determined by three satellite ocean color sensors (MERIS, SeaWiFS and MODIS-A) at an offshore site in the Mediterranean Sea (BOUSSOLE project), Journal of Geophysical Research, 113, C07013, doi:10.1029/2007JC004472.

Zibordi, G., F. Mélin, and J.-F. Berthon, Comparison of SeaWiFS, MODIS and MERIS radiometric product at a coastal site (2006), Geophysical research letters, vol 33, L06617, doi: 10.1029/2006GL025778

MERMAID, the MERIS Matchups In situ Dabase http://hermes.acri.fr/mermaid

B. A. Franz, S. W. Bailey, P. J. Werdell and Ch. R. McClain, Sensor-independent approach to vicarious calibration of satellite ocean color radiometry, Applied Optics 46, No 22, 5068 —5082 (2007).

S. W. Bailey, S. B. Hooker, D. Antoine, B. F. Franz, P. J. Werdell, Sources and assumptions for the vicarious calibration of ocean color sensors, Applied Optics 47, No 12, 2035– 2045 (2008).

H. Gordon, In-orbit calibration strategy for ocean color sensors, Remote Sensing of Environment, 63, 265—278 (1998).

C. Lerebourg, C. Mazeran, J.-P. Huot, D. Antoine, Vicarious adjustment of the MERIS Ocean Colour Radiometry and in situ validation on the MERMAID database, MERIS ATBD-2.11, 2011 (Issue 1, rev.0)

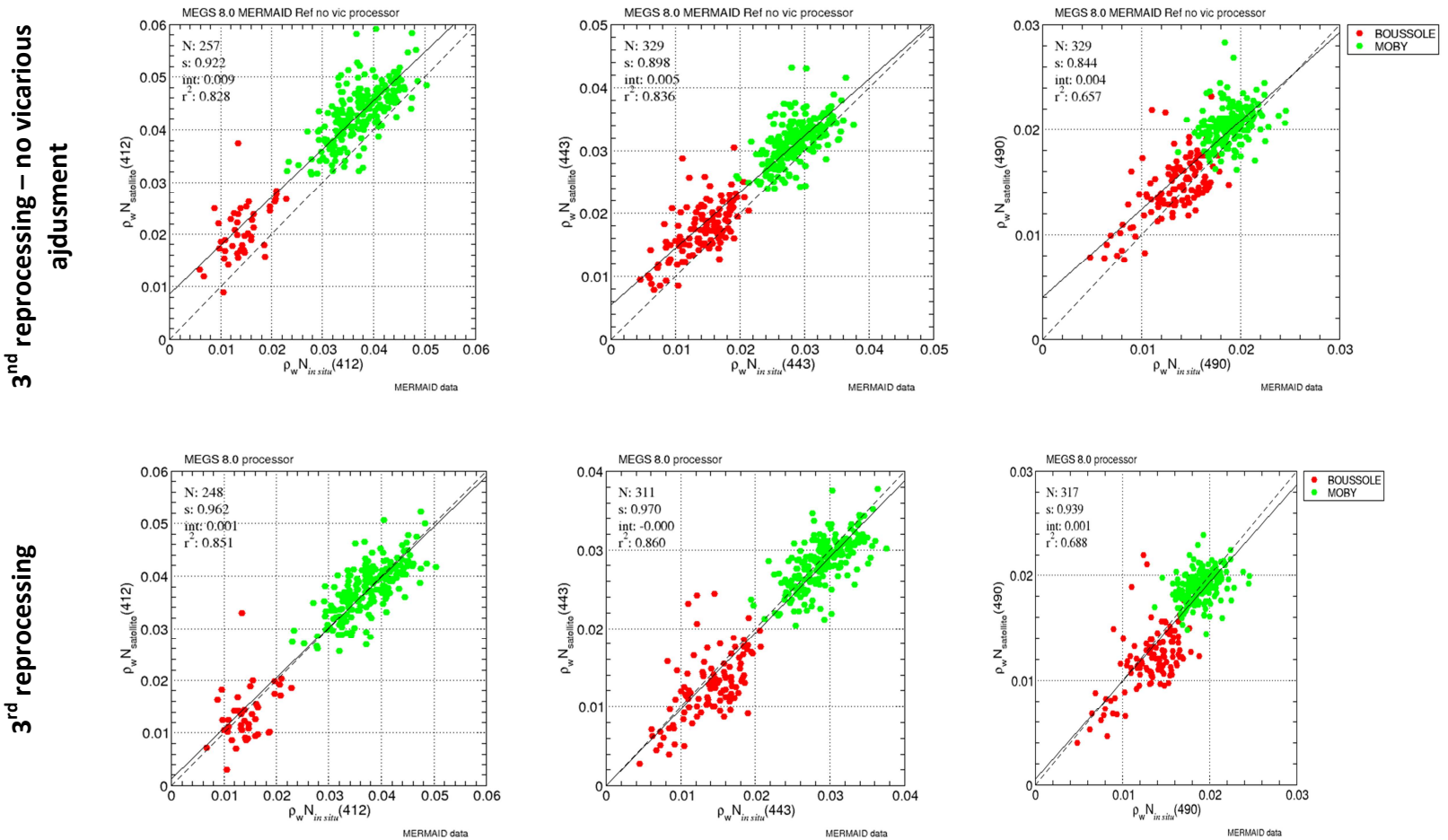

Figure 13: Scatterplots of MERIS versus in-situ fully normalized water leaving reflectances at 412 nm (left), 443 (middle) and 490 nm (right) for the 3rd reprocessing without vicarious adjustment (top) and 3rd reprocessing with vicarious adjustment (bottom).

6.3 Bright Pixel Atmospheric Correction (BPAC)

Contributors: Gerald Moore (Bio-optica)

Purpose and description of changes

The BPAC has been substantially revised with a complete rewrite of the code. The algorithm has been extended to address a number of potential issues that were found in the previous version.

Implemented changes:

Full details of the changes are beyond the scope of this document and are described in [*Moore and Lavender, 2009*]. Specifically the following changes have been introduced:

1. The algorithm is now specified in terms of Inherent Optical Properties (IOP) rather than nominal Total Suspended Matter (TSM) load;
2. The variation of f/Q is now accounted for in the algorithm;
3. The f/Q has been implemented in tables at MERIS geometry and for waters ranging from pure water to a maximum single scattering albedo of 0.9999;
4. The BPAC returns the values of pure water on failure;
5. Particulates are flagged as 'white' (*e.g.*coccoliths) or absorbing;
6. Specific absorption has been estimated for now white particulates;
7. The BPAC now tests for non-convergence of the iterative process;
8. The BPAC now uses the 885 nm band to extend its dynamic range;

Impact, expected change on product

At high turbidities, the BPAC uses longer NIR wavelengths to extend its dynamic range. Figures below show $\rho_w(560)$ retrieved from the 2nd reprocessing (Figure 14) and the 3rdreprocessing (Figure 15). The BPAC now performs over the mouth of the Amazon and produces realistic $\rho_w(560)$ values without atmospheric correction failure.

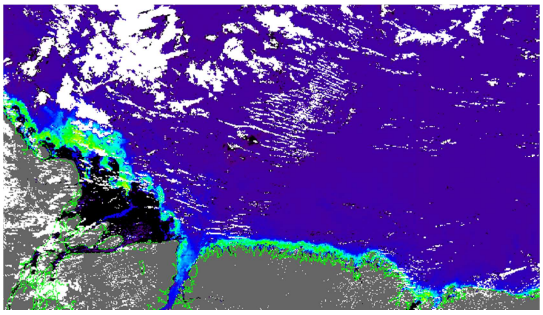

Figure 14: $\rho_w(560)$ retrieved from the 2nd reprocessing

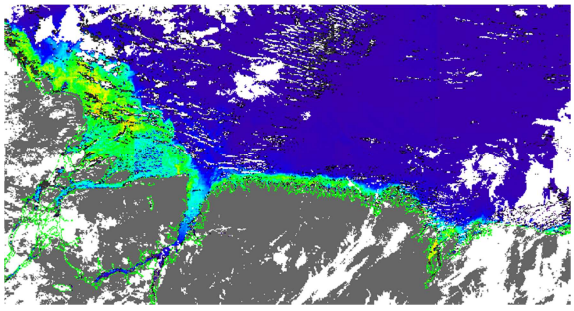

Figure 15: $\rho_w(560)$ retrieved from the 3rd reprocessing

The figure below shows the reflectance retrieved at 709 nm from the 2nd vs. 3rd reprocessing along a transect Figure 16which covers a range from low to medium turbidity waters. The regression Figure 17shows that the relationship is close to 1:1 and for medium turbidity waters there should be no difference in the performance and results from the BPAC.

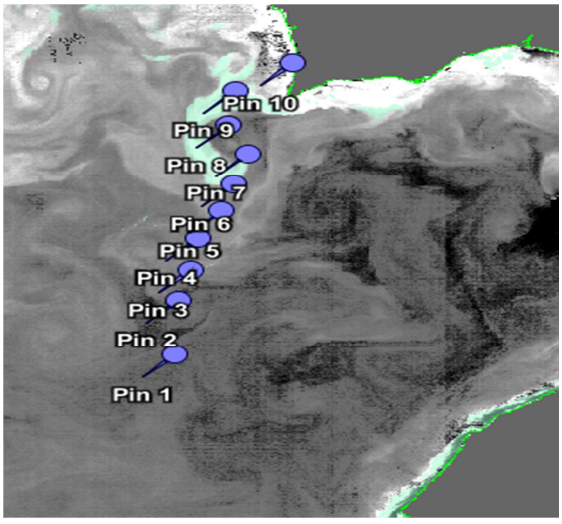

Figure 16: Turbidity range of data extracted and plotted in Figure 17

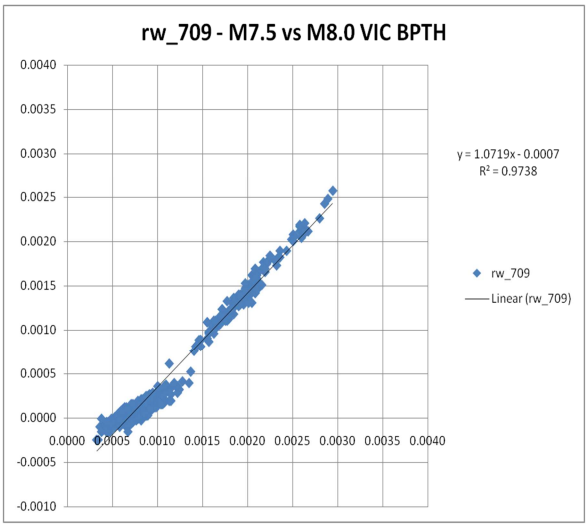

Figure 17: Regression between 709 nm reflectance retrieved from2nd and 3rd reprocessing

Figure 18shows the TSM derived from the BPAC (intermediate product), for the River Plate. The BPAC now functions over the full range of TSM up to an estimate maximum of 500 $g.m^{-3}$. The estimated TSM values are obtained from the b_b conversion for sediment in the MERIS Reference Model Documents [Barker 2009].

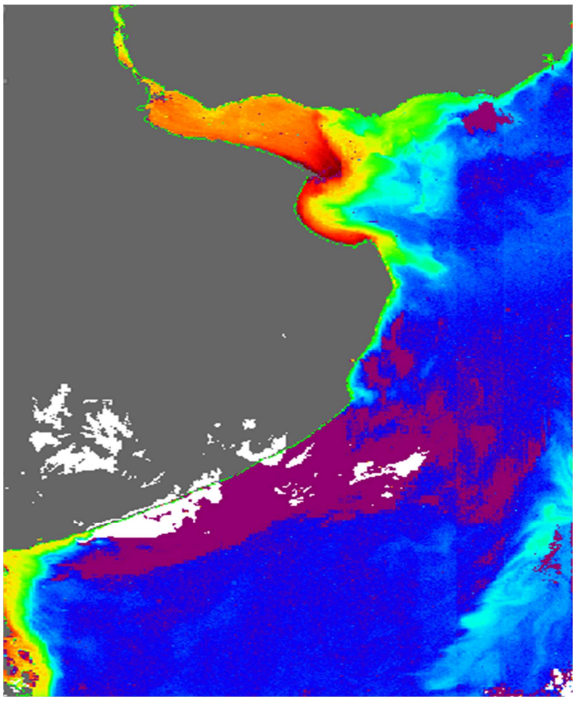

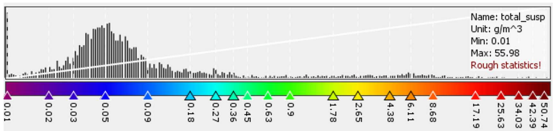

TSM range x0.1 i.e. 0.1 … 500 g.m^{-3}

Figure 18: TSM derived from the BPAC

Issues not addressed in the 3rd Reprocessing

- Adjacency: The BPAC is sensitive to the effects of near coastal adjacency, especially where there are low to medium turbidity water near shore. The algorithm as implemented in ODESA performs considerably better when coupled with ICOL (*Santer & Zagolski 2008*); this solution is available but is outside the scope of the reprocessing;
- Glint: The BPAC relies on the standard glint correction, and data should be interpreted with caution in the high glint regions in low turbidity waters.

Reference

Moore G. and S. Lavender, MERIS ATBD 2.6 –Case 2-S Bright Pixel Atmospheric Correction – Version 2009

Santer, R. and F. Zagolski, 2008, ICOL – Improved Contrast between Ocean and Land, ATBD MERIS Level1-C, version 1.1.

K. Barker, Reference Model for MERIS Level2 Processing: third MERIS Reprocessing, Doc. no PO-TN-MEL-GS-0026, July 2009

6.4 Radiative transfer LUTs and interpolations

6.4.1 Rayleigh LUTs

Contributor: Francis Zagolski (ParBleu)

Purpose and description of changes

In the atmospheric correction scheme over ocean, the path radiance at Top Of Atmosphere (TOA) is corrected for the molecular scattering. Rayleigh reflectances at the 15 MERIS wavelengths are pre-computed in a LUT for a standard surface pressure over wind-roughened black sea surfaces. These computations were initially completed for a set of 2 wind-speeds (1.5 and 7.2 m/s) with the RTC/FUB (MOMO, Matrix Operator MethOd).

For the 3rd reprocessing, the Rayleigh LUT has been regenerated with a vector code (the RTC/SO - Successive Orders of Scattering (SOS) code) as:

1. The polarization has to be accounted for in the radiative transfer computation;
2. A 3rd wind-speed corresponding to a larger surface roughness level is required (now 1.5, 5.0 and 10 m/s).

Impact, expected change on product

Polarization processes impact on the TOA Rayleigh radiance computations up to few percents in relative value. This was clearly illustrated by the works from *Zagolski et al.(2004, 2006)*, in which both the polarization by the atmospheric molecules and by the Fresnel reflection of sea surface may introduce biases up to 2% (*resp.*, 3%) in relative value at 442.5 nm (*resp.*, 865 nm) for observations in the perpendicular directions to the solar plane, as illustrated by Figure 19.

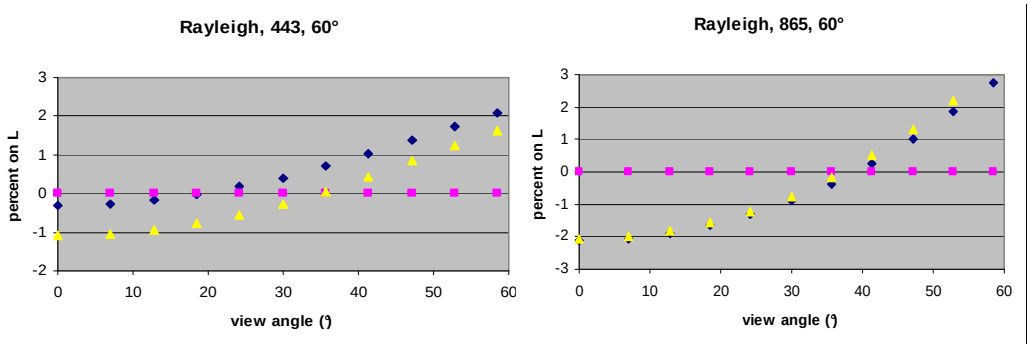

Figure 19: Relative percentage difference between the fully polarized Rayleigh radiance (molecules + Fresnel polarization) and the case of (left) a partially polarized radiance by the molecules only (yellow triangles) and (right) an unpolarized radiance (blue diamonds). These computations have been completed over a wind-roughened black sea surface (7.2 m/s) for a solar zenith angle (SZA) of 60 deg. and in the perpendicular plane to the solar plane at 442.5 nm (left) and 865 nm (right).

Of course, such biases impact directly on the retrieval of the water-leaving radiance.

Moreover, the new set of 3 wind-speeds (1.5, 5 and 10 m/s) used in the Rayleigh LUT for the 3rd reprocessing allowed to solve the large discrepancies (~1.6%) initially observed for the large viewing zenith angles between the extrapolated Rayleigh reflectance and the exact computation in the case of wind-speeds larger than 7.2 m/s.

References

Zagolski, F., and R. Santer, 2004. Polarization effect in radiative transfer computation within a coupled Atmosphere-Land/Ocean system, *PARBLEU Report (PO-RP-PAR-GS-0001-1B): 'ADEOS-II Ground Segment for GLI'*, Quebec (Qc), Canada, April 2004: 75 p.

Zagolski, F., R. Santer, J.P. Huot, and M. Bouvet, 2006.Impact of polarization effect in MERIS look-up tables over black oceans, *PARBLEU/LISE/ESA Presentation at the MERIS DQWG #11*, ESA/ESRIN, Frascati - Italy, September 11-12 2006.

6.4.2 Aerosols LUTs

Contributors:Francis Zagolski (ParBleu)

Purpose and description of changes

Accuracy of the atmospheric correction is directly related to the ability of the aerosol model to well describe the spectral dependence between the near-infrared (NIR) and the blue region. This purpose is well illustrated in the works from *Gordon et al.* (1996). The set of blue aerosols (Junge models) used in the 2ndreprocessing yielded to unsatisfying atmospheric correction (whiter than expected)and have been redefined for the 3rd reprocessing. The approach consisted in combining the micro-physical properties of these small particles with their Inherent Optical Properties (IOPs) derived from CIMEL measurements acquired over oceanic sites [*Santer andZagolski, 2006*]. A set of 3 new blue IOP models has then been substituted to the Junge models in the previous set of Standard Aerosol Models (SAMs).

For the atmospheric corrections, the radiative properties of the aerosols (16 SAMs + 18 DUSTs) are stored in pre-computed LUTs to speed-up the algorithms implemented in the MERIS ground segment(see [*Zagolski, 2011(a, b)]* for more details). For the 3rd reprocessing, these LUTs have been generated for a set of 6 AOTs (at 550 nm) for the boundary/dust aerosols against 5 AOTs in the 2nd reprocessing. The additional AOT of 0.01 was included in order to improve the 2nd order polynomial fit expressing the ratio (ρ_{path}/ρ_R) as function of the total AOT, towards the point corresponding to the pure Rayleigh case (AOT=0, ρ_{path}/ρ_R=1). Moreover, for the same reasons as specified for the Rayleigh table, the LUT of polynomial coefficients (ρ_{path}/ρ_Rvs AOT) has been generated with the SO vector code to include the polarization processes for the 16 SAMs only (MOMO being used for the DUSTs), using the new set of 3 wind-speeds (both for the SAMs and the DUSTs), *i.e.* 1.5, 5.0 and 10 m/s. These polynomials have been quality checked before to be implemented for the 3rd MERIS reprocessing.

Impact, expected change on product

As depicted in Figure 20, the Junge models do not reproduce accurately the spectral dependence for the small particles. While the normalized extinction coefficient, $\sigma_e(\lambda,\alpha)/\sigma_e(550,\alpha)$ is overestimated with these Junge models for the short wavelengths, the latter is slightly underestimated for larger wavelengths toward the NIR region. Moreover, the retrieved Aerosol Phase Functions (APFs) from CIMEL measurements at 440 nm for these small particles display a deviation in the backscattering region (Figure 21). The blue aerosols being mono-dispersed sub-micro particles, the absence of large particles reduces the backscattering. The overestimate of blue aerosol phase functions with the Junge model implies an underestimate of the AOT at 440 nm and impacts directly on the MERIS aerosol product over oceans. Thank to this better description of the spectral dependence of this new set of blue IOP models, some improvements are expected in the derived aerosol products, *i.e.* in the identification of these small particles and their associated AOT at 865 nm.

In the 3rd reprocessing, the implementation of an additional quality test (*i.e.*, assuming the unique solution when inverting the polynomial within the AOT range) on the establishment of the 2nd order polynomial fits, should ensure a better confidence in the retrieved aerosol product.

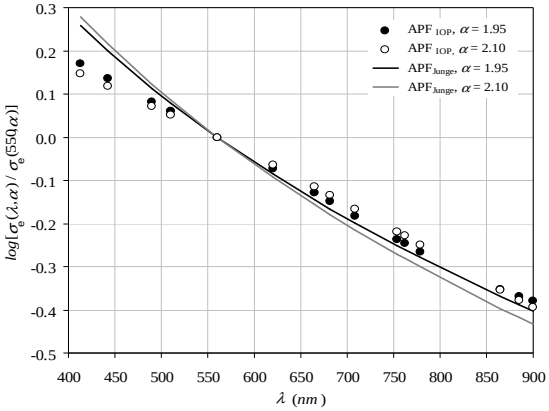

Figure 20: Spectral dependence of the normalized extinction coefficients ($\sigma_e(\lambda,\alpha)/\sigma_e(550,\alpha)$) for the blue aerosol models (α=1.95 and 2.10). Full lines correspond to the Junge models and circle symbols are for the IOP models.

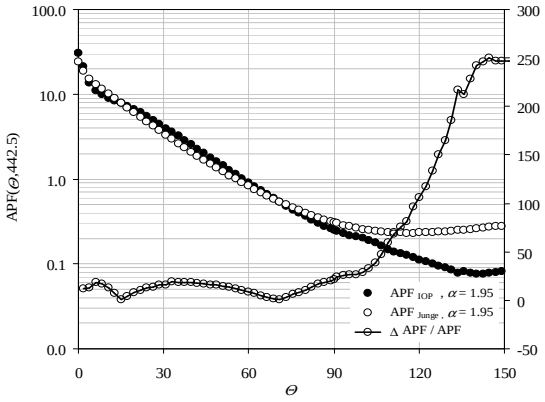

Figure 21: Comparison between the average value of APFs extracted at 442.5 nm from the CIMEL measurements over all the oceanic sites from AERONET, and the APF associated with the Junge model ($\alpha \geq 1.95$).

Of course, all these improvements in the generation of ocean-aerosol LUTs directly impact on the retrieval of marine reflectance.

References

Gordon, H.R., and T. Zhang, 1996. How well can radiance reflected from the ocean-atmosphere system be predicted from measurements at the sea surface, *Applied Optics*, 35 (33), pp. 6527-6543.

Santer, R., and F. Zagolski, 2006. Inherent optical properties of the aerosols – IOPA, in reponse to RFQ/3-11641/06/I-OL, Intended Rider 1 to ESRIN Contract 18109/04/I-OL for Atmospheric Correction for MERIS Over Coastal Waters: Towards a New Aerosol Climatology: 40 p.

Zagolski, F, 2011*a*. Specification of the contents of the MERIS radiative transfer tools used to generate the level-2 auxiliary data products, *PARBLEU/ESA Report (PO-RS-PAR-GS-0002-3C): 'ENVISAT-1 Ground segment for MERIS'*, Quebec (Qc), Canada, Feb. 2011: 142 p.

Zagolski, F, 2011*b*. Specification of the scientific contents of the MERIS level-1b & 2 auxiliary data products, *PARBLEU/ESA Report (PO-RS-PAR-GS-0002-3C): 'ENVISAT-1 Ground segment for MERIS'*, Quebec (Qc), Canada, Feb. 2011: 540 p.

6.4.3 Transmittance LUTs

Contributors: Francis Zagolski (ParBleu), Marc Bouvet (ESA)

Purpose and description of changes

Until the 3rd MERIS reprocessing, the total downward and upward transmittances of the atmosphere (Rayleigh + aerosol components) required in the final step of the atmospheric correction algorithm over case-1 waters, were approximated by an analytical formulation from *Gordon and Wang* (*see* MERIS ATBD-2.7, issue 5 - rev.0, 2005).

A new set of LUTs with total (direct + diffuse) upwelling and downwelling atmospheric transmittances, fully in line with the atmospheric correction algorithm over oceans, was generated and integrated in the MERIS 3rd reprocessing.

Impact, expected change on product

The MERIS water-leaving reflectance (ρ_w) comes from the removal of the path atmospheric reflectance (ρ_{path}) to the TOA reflectance (ρ^{TOA}) (itself first corrected for gaseous absorption, smile effect and glint reflectance):

$$\rho_w^{TOA} = \rho^{TOA} - \rho_{path} = T_u \cdot T_d \cdot \rho_w$$

Where T_u and T_d are the total upwelling and downwelling atmospheric transmittances. In the 2nd reprocessing, these transmittances were approximated by:

$$T_u(\mu) = T_d(\mu) = T_R(\mu) \cdot T_a(\mu) = \exp\left[-\frac{1}{\mu} \cdot \left(\frac{\tau_R}{2} + (1 - \omega_a \cdot f_a) \cdot \tau_a\right)\right]$$

in which:

- T_R and T_a are the Rayleigh (molecules) and aerosol transmittances;
- τ_R and τ_a are the Rayleigh and aerosol optical thicknesses;

- ω_a and f_a are the single scattering albedo and the forward scattering proportion of the aerosols;
- μ is the cosine of zenith angle.

This above formulation of total atmospheric transmittance [*Gordon and Wang, 1994*] remains an approximation which increasingly departs from an exact solution (as computed in the transmittance LUTs of the 3rd reprocessing) as the solar or view zenith angle (SZA or VZA) increases and with increasing turbidity of the atmosphere. Errors on one-way transmittances were found to be significant in the first MERIS bands (> 5%) with SZA > 60° (Figure 22).

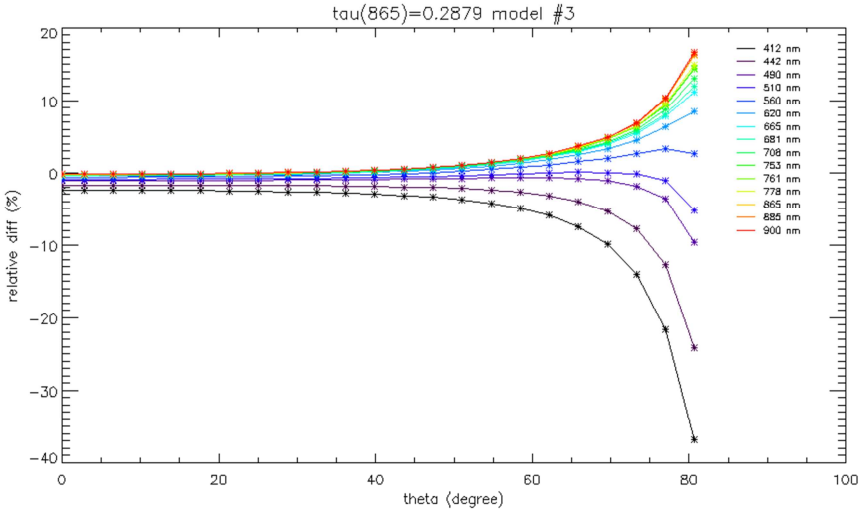

(a)

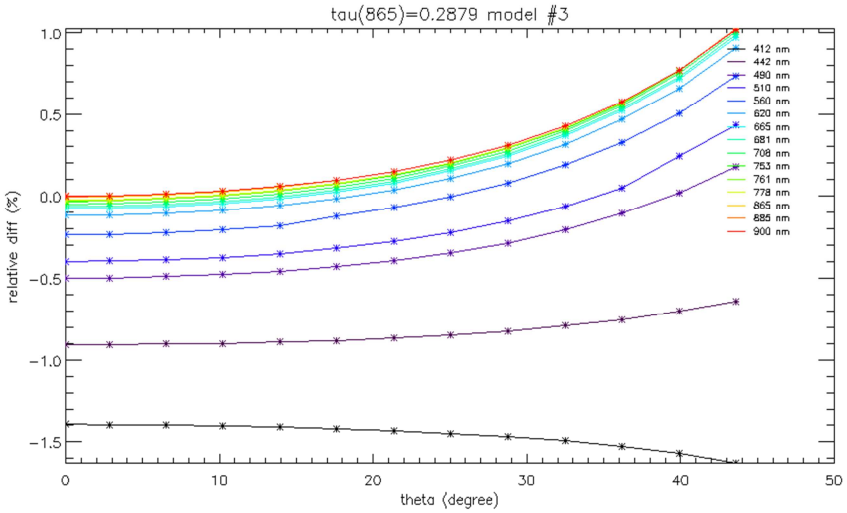

(b)

Figure 22: Relative percentage difference between total (Rayleigh+aerosol) transmittances estimated with Gordon & Wang formulation and extracted from LUTs (3rd MERIS reprocessing) at the 15 MERIS wavelengths for SAM #3 (MAR90+CONTI+H2SO4): (a) downwelling transmittances (T_d), and (b) upwelling transmittances (T_u).

Such difference between the analytical formulation of the 2nd reprocessing and the transmittance LUTs of the 3rd reprocessing partially explains the decrease of several tens of

percent in water-leaving reflectances observed at high latitude in winter (large SZA) as observed on the two level-3 products in Figure 23.

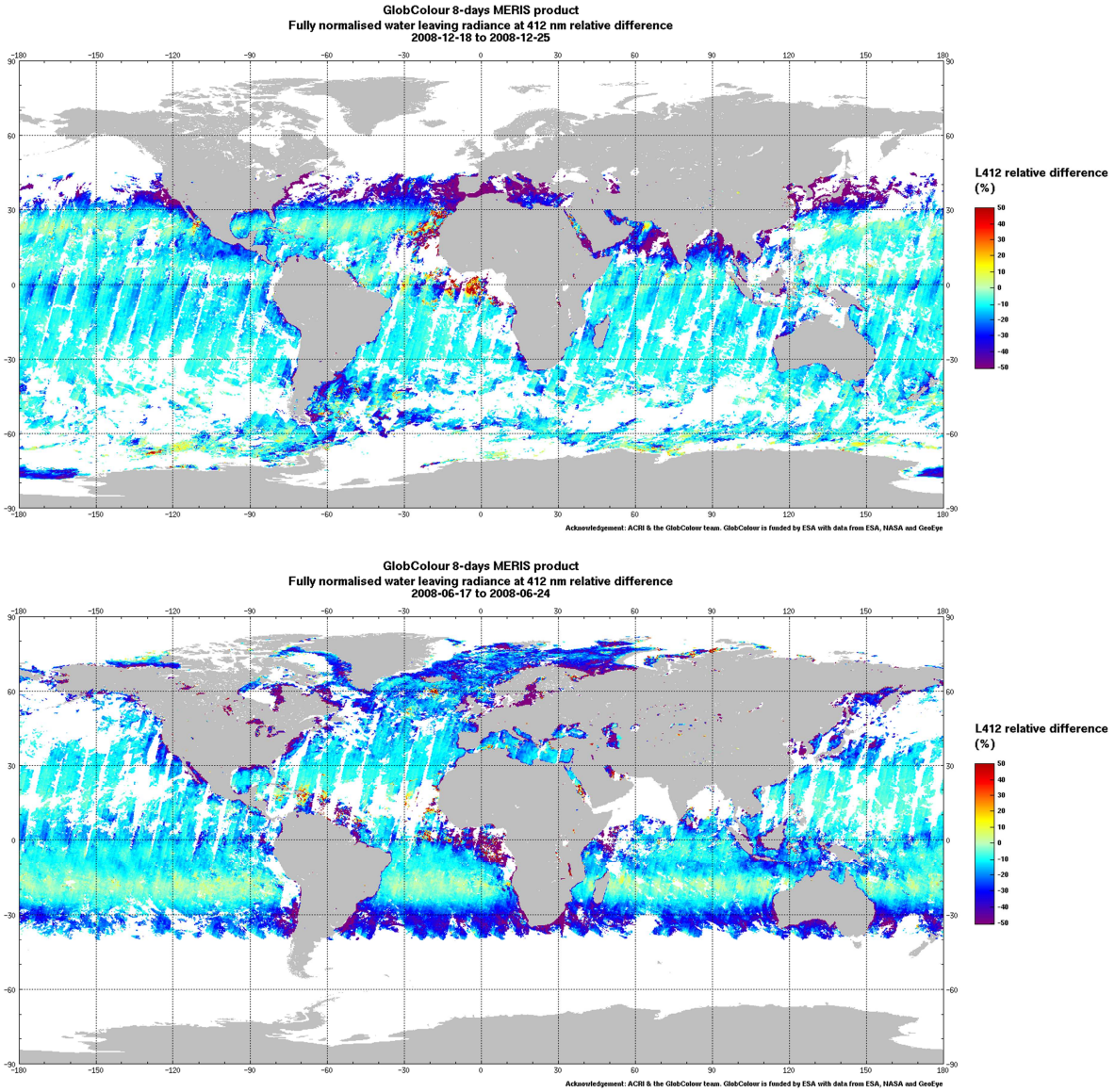

Figure 23: Differences in percentage between the fully normalized water-leaving reflectances from the 2nd reprocessing (reference) and the 3rd reprocessing for 2 different periods of 8 days.

References

MERIS ATBD-2.7 (Issue 5, rev.0), 2005. Atmospheric correction of the MERIS observation over ocean Case-1 waters (Antoine et *al.*, 2005).

Gordon, H.R., and M. Wang, 1994.Retrieval of water-leaving radiances and aerosol optical thickness over the oceans with SeaWiFS: A preliminary algorithm, *Applied Optics*, *33* (3), pp. 443-452.

6.4.4 Interpolation

Contributors: Francis Zagolski (ParBleu) and Constant Mazeran (ACRI-ST)

Purpose and description of changes

In order to keep the full accuracy in radiative transfer computation, both Rayleigh and polynomial coefficients (ρ_{path}/ρ_R vs. AOT) LUTs have been generated with a specific grid in (θ_s, θ_v, $\Delta\phi$) and in AOTs (7 values including the pure Rayleigh case). Some multi-linear interpolations are then needed to extract from these LUTs the atmospheric parameters (reflectance, transmittance) for the specific MERIS data acquisitions.

Compared with the 2nd reprocessing, the main change consisted in applying an angular interpolation in cosine of zenith angle ($\mu = \cos\theta$) on the atmospheric parameters extracted from these LUTs. The latter has been selected to reduce the errors induced by the interpolation on these atmospheric parameters.

The second change refers to the numerical inversion the aerosol optical thickness (τ^a) from the ratio of path to Rayleigh reflectance ($\xi=\rho_{path}/\rho_R$). The relation between both quantities is approximated by a second order polynomial, for any sun/view geometry, wavelength and aerosol model [*Antoine and Morel, 1999*]. Now, we firstly interpolate and store the polynomial coefficients, instead of the polynomial estimate, in order to consider the same polynomial between computations of ξ (direct) and τ^a (inverse).

Impact, expected change on product

The impact on the L2 water-leaving reflectance should be minor.

References

Antoine, D., and A. Morel, 1999. A multiple scattering algorithm for atmospheric correction of remotely sensed ocean color (MERIS instrument): Principle and implementation for atmospheres carrying various aerosols including absorbing ones, *International Journal of Remote Sensing*, 20 (9), pp. 1875-1916.

6.5 Level2 output marine reflectance in the NIR

Contributors: Gerald Moore (Bio-Optika), Constant Mazeran (ACRI-ST)

Purpose and description of changes

Because the atmospheric correction of [*Antoine and Morel, 1999*] is based on the black pixel assumption at 779 and 865 nm, the MERIS scheme first removes the marine residual signal $t\rho_w$ detected by the BPAC in the near infrared for identifying aerosol type and quantity. Although the method should theoretically retrieve, after path reflectance correction, the BPAC $t\rho_w$ at 779 and 865 nm, numerical uncertainties and non-bijective numerical operations generate errors. For the 3rd reprocessing is has thus been decided to directly write the marine signal of the BPAC in the Level 2 products.

Impact, expected change on product

Level 2 products now include the direct outputs of the BPAC at bands 779, 865 and 885 nm, corrected for the Rayleigh and aerosol transmittance retrieved by atmospheric correction (t_{up} and t_d):

$$\rho_w(\lambda) = \frac{t\rho_{wC2}(\lambda)}{t_{up}(\lambda)t_d(\lambda)} \quad for\ \lambda = 779,865,885nm$$

In particular the marine reflectance at 885 nm is no longer set to zero.

It should be reminded here that the $t\rho_w$ can be equal to the signal of pure sea water in case of BPAC failure (see dedicated section).

Note that at 709 nm the marine reflectance is still computed as

$$\rho_w(\lambda) = \frac{\rho_{gc}(\lambda) - \rho_{path}(\lambda)}{t_{up}(\lambda)t_d(\lambda)}\ for\ \lambda \neq 779,865,885nm\,.$$

Where ρ_{gc} is the TOA signal corrected for gas, smile and glint, and ρ_{path} is the path reflectance retrieved by the atmospheric correction. This equation is also true at 753 nm since there is no $t\rho_w$ output of the BPAC at that band.

References

Antoine, D. and A. Morel, 1999. A multiple scattering algorithm for atmospheric correction of remotely sensed ocean color (MERIS instrument): Principle and implementation for atmospheres carrying various aerosols including absorbing ones, *International Journal of Remote Sensing*, 20 (9), pp. 1875-1916.

See also dedicated section on BPAC above.

6.6 Algal pigment index retrieval (chl1)

6.6.1 OC4Me

Contributors: David Antoine (LOV)

Purpose and description of changes

The OC4Me algorithm (Morel et al., 2007a) was adopted for the retrieval of the MERIS "Case-1 waters pigment index" (hereafter simply referred to as "Chl") in an effort to incorporate latest field data from recent cruises [*PROSOPE, Claustre et al., 2002. BENCAL, Morel et al., 2006. AOPEX, Morel et al., 2007b. BIOSOPE, Claustre et al., 2008]*. Therefore, the bio-optical model is unchanged in its construction *[Morel, 1988; Morel and Maritorena, 2001]* but relies on a more extensive data set incorporating in particular more values in both extremes of the Chl range (in particular: very low values from the BIOSOPE cruise in the Southeast Pacific gyre, and high values from the BENCAL cruise in the Benguela current system). The OC4Me algorithm and the previous MERIS algorithm are based on this bio-optical model.

The previous MERIS Chl algorithm switched from using the 443/560 to the 490/560 and to the 510/560 band ratios based on two Chl thresholds, i.e., Chl< 0.1 and Chl< 1 mg m-3. The OC4Me algorithm generalizes this concept by using the maximum of these three band ratios, without relying on a threshold in terms of Chl concentration.

This technique is referred to as a "Maximum Band Ratio algorithm" (MBR), which is the principle of the OC4V4 algorithm used for SeaWiFS, for instance *[O'Reilly et al., 1998, 2000]*.

As said above, the second change originates from updating the data base onto which the bio-optical model is built. This model uses a Chl-based formalism to express the diffuse attenuation coefficient for downward irradiance, Kd, as follows:

$$K_d(\lambda) = K_w(\lambda) + \chi(\lambda)\, Chl^{e(\lambda)}$$

where Kw(λ) is the pure seawater contribution to Kd(λ), and the χ(λ) coefficients and the e(λ) exponents are derived from a data base of concurrent field measurements of Chl and Kd(λ). Irradiance reflectances R (ratio of the upward to the downward plane irradiance just beneath the sea surface) are derived from the Kd values following the procedure described initially in *[Morel, 1988]* and also detailed in *[Morel and Maritorena, 2001]*.

The χ(λ) coefficients and the e(λ) exponents have been slightly revised after the incorporation of new field data (see Fig. 4a in *[Morel et al., 2007a]*). These χ(λ) and e(λ) values are available on the internet at: ftp (oceane.obs-vlfr.fr, cd pub/morel, file e_chi_Kw_2006).

It is worth noting that the Kd-Chl relationship derived from this data set is fully compatible with the relationship derived from using the NOMAD *[Werdell and Bailey, 2005]* data set (Fig. 4 in *[Morel et al., 2007a]*).

The OC4Me algorithm is eventually expressed as a polynomial:

$$\log_{10}(Chl) = a_0 + \sum_{n=1}^{4} a_n \log_{10}(R_i^j)^n$$

where

$$R_i^j = \max\left(R_{443}^{560}, R_{490}^{560}, R_{510}^{560}\right)$$

The a_0 to a_4 coefficients are presented in Table 10 (from Table 2 in *[Morel et al., 2007a]*):

Table 10: Polynomial coefficients of the OC4Me [Morel et al., 2007a]

a_0	a_1	a_2	a_3	a_4
0.4502748	−3.259491	3.522731	−3.359422	0.949586

Impact, expected change on product

By construction, the expected impact as compared to the previous MERIS algorithm and to OC4V4 (SeaWiFS) is to produce lower Chl for low values, say below about 0.2 mg m^{-3}, and slightly higher Chl values in the upper part of the Chl range, above about 1 mg m^{-3}. Between these two values the change is much smaller (Fig. 2 in *[Morel et al., 2007a]*, reproduced below - Figure 24).

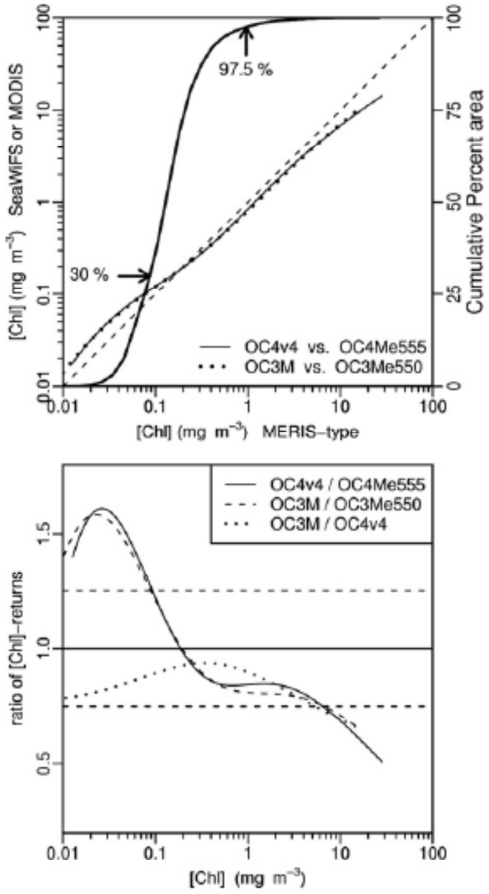

Fig. 2. Inter-comparison of the [Chl] returns. a) Returns (ordinates) of OC4v4 (SeaWiFS) and OC3M (MODIS-A), compared to the [Chl] values (abscissae), as returned by their companion MERIS-algorithms (OC4Me-555 and OC3Me-550). Note that the returns from OC4Me, OC4Me-555 and OC3Me-550, strictly follow the 1-to-1 line, because these algorithms are derived from the same bio-optical model, and thus are totally redundant. Also shown (heavy line, linear right ordinate scale as %), the cumulative frequency of occurrence within the world ocean of pixels with increasing [Chl] values (mean annual values; data from SeaWiFS; reproduced from Fig. 8 in Antoine et al., 2005), b). Ratio of the paired algorithms outputs as a function of [Chl] which is returned by the algorithm appearing in the denominators (see inset); the horizontal lines show ratios equal to 1.25, 1, and 0.75. The polynomial expressions for these curves are available on request.

Figure 24: Figure 2 in [Morel et al. 2007a]. Note that OC4Me555 used here is a modified version of OC4Me, using the 555nm band of SeaWiFS instead of the 560nm band of MERIS.

The impact is shown also in Figure 25, from the comparison between Chl estimates from OC4Me and from the previous MERIS algorithms, when both are applied on the same set of reflectance spectra from the MERMAID data base (reflectances determined from field radiometric measurements).

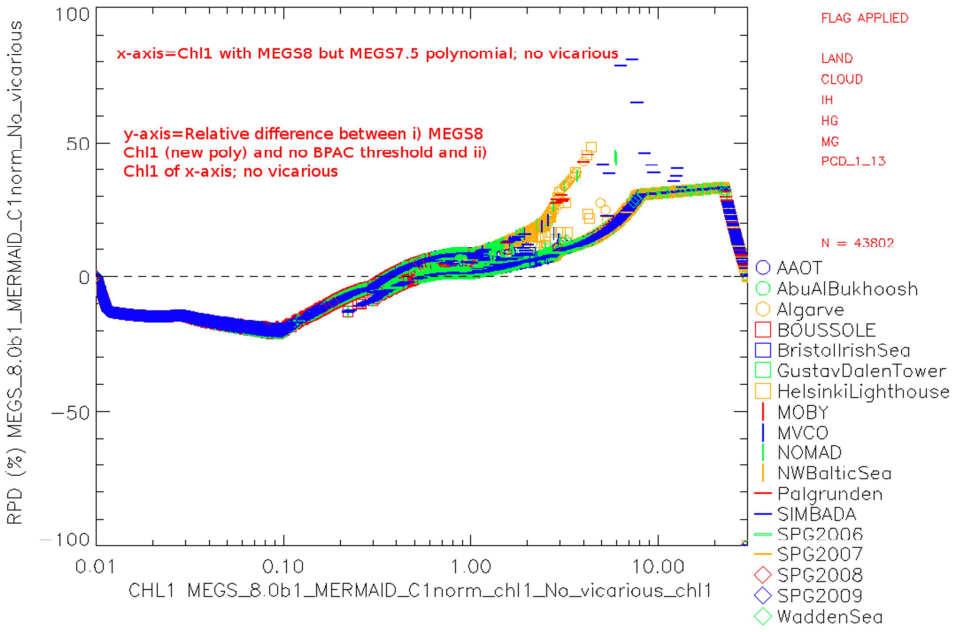

Figure 25: Relative difference (in percents) between the Chl concentration produced by the OC4Me and by the previous MERIS algorithm, when both are applied to the same set of reflectance spectra from MERMAID (including both Case 1 and Case 2 waters).

References

Claustre, H., Morel, A., Hooker, S.B., Babin, M., Antoine, D., Oubelkheir, K., Bricaud, A., Leblanc, K., Quéguiner, B. and S. Maritorena, 2002. Is desert dust making oligotrophic waters greener? Geophysical Research Letters, 29, 1469, 10.1029/2001GL014056.

Claustre, H., Sciandra A., and D. Vaulot, 2008. Introduction to the special section Bio-optical and biogeochemical conditions in the South East Pacific in late 2004: the BIOSOPE program. Biogeosciences, 5, 679-691.

Morel, A., 1988.Optical modeling of the upper ocean in relation to its biogenous matter content (case 1 water), Journal of Geophysical Research, 93, 10,749-10,768.

Morel, A., Claustre, H., Antoine, D. and B. Gentili, 2007b. Natural variability of bio-optical properties in Case 1 waters: attenuation and reflectance within the visible and near-UV spectral domains, as observed in South Pacific and Mediterranean waters. Biogeosciences,4, 913-925

Morel, A., Gentili, B., Chami, M., and J. Ras, 2006. Bio-optical properties of high chlorophyll Case 1 waters, and of yellow-substance- dominated Case 2 waters. Deep-Sea Research I, 53, 1439-1559

Morel A., Y. Huot, B. Gentili, P.J. Werdell, S.B. Hooker, and B. A. Franz, 2007a. Examining the consistency of products derived from various ocean color sensors in open ocean (Case 1) waters in the perspective of a multi-sensor approach, Remote Sensing of Environment 111, 69–88.

Morel, A., and S. Maritorena, 2001. Bio-optical properties of oceanic waters: A reappraisal. Journal of Geophysical research, 106, 7763-7780.

O'Reilly, J. E., Maritorena, S., Mitchell, B. G., Siegel, D. A., Carder, K. L., Garver, S. A., et al. (1998). Ocean color algorithms for SeaWiFS.Journal of Geophysical Research, 103, 24937–24953.

O'Reilly, J. E., Maritorena, S., Siegel, D. A., O'Brien, M. C., Toole, D., Mitchell, B. G., et al. (2000). Ocean color chlorophyll a algorithms for SeaWiFS, OC2, and OC4: version 4. SeaWiFSpostlaunch calibration and validation analyses, Part 3, NASA/TM 206892, Vol. 11 (pp. 9−23).

Werdell, P. J., & Bailey, S. W., 2005.An improved in-situ bio-optical data set for ocean color algorithm development and satellite data product validation.Remote Sensing of Environment, 98, 122−140.

6.6.2 Bidirectional f/Q table with Raman

Contributors: David Antoine (LOV)

Purpose and description of changes

This change was actually already incorporated in the second MERIS reprocessing, yet it was not documented.

The f/Q table is used for normalization of marine reflectances. This is an internal correction step performed when applying the OC4Me algorithm (to transform directional reflectances into irradiance reflectances).

The incorporation of a new f/Q table aims at using the latest, a priori more realistic, parameterization of the bidirectionality, including not only Raman scattering but also a Chl-varying volume scattering phase function. This f/Q modelling is fully described in Morel et al. (2002).

Impact, expected change on product

No major impact is expected, because the OC4Me uses blue and green bands where Raman scattering is negligible or moderate, and also because the OC4Me uses band ratios.

References

Morel, A., Antoine, D. and B. Gentili, 2002. Bidirectional reflectance of oceanic waters: Accounting for Raman emission and varying particle phase function, Applied Optics, 41, 6289-6306.

6.7 Case2 Branch (Case2 Regional Neural Net)

Contributor: Roland Doerffer (HZG)

Purpose and description of changes

Major change in the case 2 water branch is the introduction of a special atmospheric correction procedure for case 2 water into the processing chain, which has been developed in the C2R and sun glint correction projects of ESA. Reason was that after introducing the vicarious adjustment, which is adapted to the case 1 water atmospheric correction, unreasonable results and errors in the retrieval of the case 2 water products (algal_2, total suspended matter and yellow substance) were observed in some coastal water areas.

Furthermore, as in previous versions of MEGS, negative reflectances occur in the blue spectral bands of MERIS under some conditions with high concentrations of suspended or absorbing material.

The new case 2 water atmospheric correction procedure is based on a neural network, which is trained with simulated reflectances. The basic idea is to associate water leaving reflectances and path reflectances with top of atmosphere reflectances for a large number of different cases of solar and viewing angles, concentrations of different aerosols, concentrations of optical components in water and wind speeds for simulated sky and sun glint. These associations are manifested in the Neural Network. 12 of the 15 MERIS bands are used: 412, 443, 490, 560, 620, 670, 681, 708 and 865 nm.

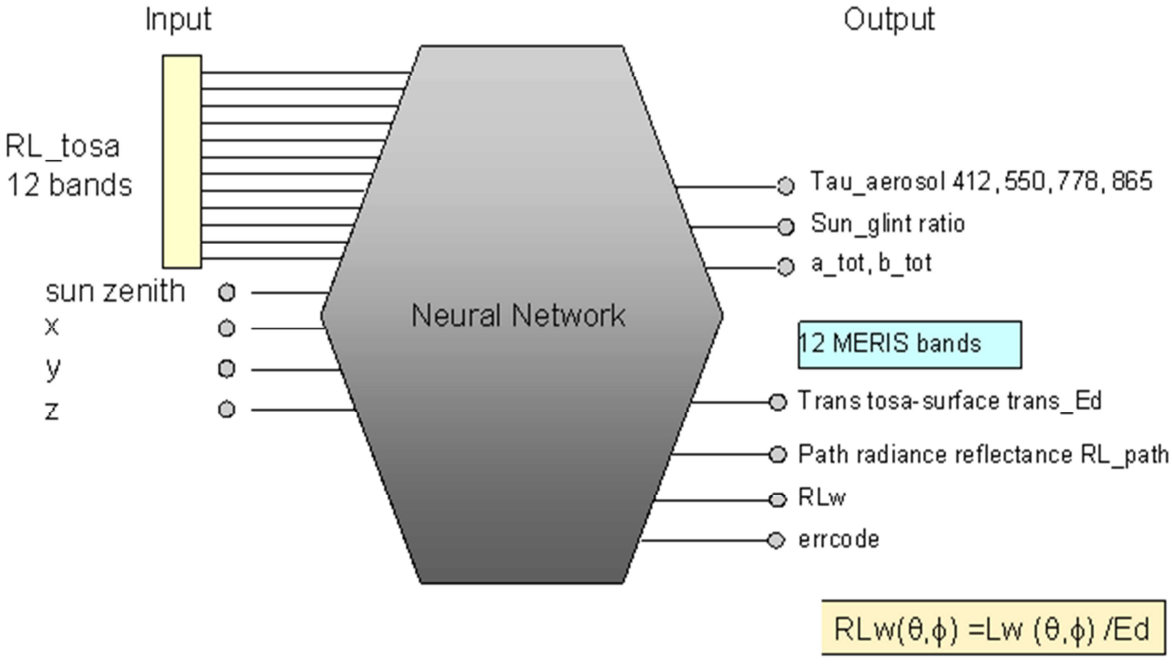

Figure 26: The Neural Network for the atmospheric correction for case 2 waters

In case of MEGS none of the outputs of the NN is provided as a product to the user and only the water leaving radiance is used *i.e.* as input to the water neural network system.

For simulating the radiative transfer in the atmosphere and the Fresnel reflectance at the water surface, the Monte Carlo photon tracing program of HZG was used and for the water leaving radiance simulations, Hydrolight. Based on these simulations, a forward neural network was trained, which was then combined with the results of the Monte Carlo simulations.

A further aspect of the atmospheric correction procedure was to retrieve also water leaving radiances over sun glint contaminated areas. This function is implicitly included in the procedure since the sun glint is part of the simulation for the training data set.

Since this type of atmospheric correction procedure cannot produce negative reflectances it is not necessary to include threshold values as it was the case in previous MEGS versions.

Impact, expected change on product

Main impact will be the gain in valid coverage of a scene, which has to be excluded and masked when using the case 1 water atmospheric correction procedure (*e.g.* negative reflectances). Furthermore, there is also a reduction in noise, due to the fact that the procedure does not require a subtraction of a computed path radiance from the top of atmosphere radiance at low water reflectance values, e.g. in the near infrared over clear case 1 water or in the blue spectral range over strongly absorbing water.

However, also the new atmospheric correction has a certain scope, which is defined by the model used to compute the training data set. The limits used in the simulations also define the test for triggering the pcd_16/17 flag.

Known issues:

- A slight angular dependency has been detected in the water leaving reflectance. It increases with decreasing wavelength and decreasing from left to right;
- Note that this above mentioned water-leaving radiance reflectance is not accessible in the MERIS Level 2 product.
- The values of the yellow substance absorption product are too low for the Baltic Sea. Possible reason is that the algorithm is not adapted to freshwater so that the simulated reflectance for training the NN is too high in particular in the blue spectral range due to the higher scattering coefficient and refractive index of salt water.
- The chlorophyll values retrieved by the NN do no go below 0.04 , when AP1 goes below 0.01
- There seems to be a problem in the glint, where chlorophyll values increase several fold on the same oligotrophic targets seen with different geometries.

6.8 Flags

6.8.1 Flag ICE_HAZE (Sea Ice)

Contributor: Carsten Brockmann (Brockmann Consult)

Purpose and description of changes

The ICE_HAZE flag indicates situations over the ocean where the pixel conditions are not suitable to retrieval water products. This can be either due to the atmosphere being too opaque (high aerosol concentration, semi-transparent cloud) or the water being frozen. However, in 2nd reprocessing explicit sea ice detection was not included. This has been added in the 3rd reprocessing. The algorithm is part of the pixel classification and described in section 4.2.3. In brief, the MERIS Differential Snow Index MDSI (based on the ratio of bands 13 and 14) is applied to pixels which have been identified as bright by one of two dedicated bright pixel detection tests.

Outside sun high glint condition, i.e. with no or medium sun glint, the ICE_HAZE flag is raised if the pixel reflectance exceeds a certain threshold (bright test) or if the above mentioned snow/ice test (MDSI) is true. A final restoration test is made; if the white scatterers are detected and the WHITE_SCATTERER flag is set to true, the ICE_HAZE flag is always set to false.

Under high glint conditions the ICE_HAZE flag is always set to TRUE. This is done in order to raise a warning (a detection of a too opaque atmosphere or sea ice is not possible, but retrieval of water products is also not possible).

Impact, expected change on product

The number of ICE_HAZE flagged pixels is substantially reduced compared with the 2nd reprocessing. The changes in the pixel classification, namely the increased number of pixels identified as clouds and the introduction of sea ice detection plus the restoration of white scatterer pixel all lead to a decrease of pixels flagged as ICE_HAZE.

References

None

6.8.2 Flag BPAC_ON

Contributor: Gerald Moore (Bio-Optika)

Purpose and description of change

In 2nd reprocessing, the BPAC flag is always raised as all pixels go through BPAC screening. No information is available whether or not the BPAC succeeded.

Definition of this flag has changed in the 3rd reprocessing: although the BPAC is still activated over all pixels, the flag BPAC_ON flag is now raised only when the correction is successful. Otherwise it means that there was a failure in the processing and in such a case the residual marine signal in the NIR is set to the one of pure sea water.

This happens in particular for very clear waters, but not only.

Hence it is worth checking the BPAC_ON flag above turbid waters for ensuring proper atmospheric correction.

6.8.3 Flag Case_2Anom

Contributors: David Antoine (LOV), Christophe Lerebourg (ACRI-ST)

Purpose and description of changes

The "Case2anom" flag is supposed to indicate where the irradiance reflectance at 560 nm is larger than the maximum value that one would expect for the actual chlorophyll concentration if the pixel would belong to the Case 1 water category. Therefore, the "Case2anom" essentially indicates the presence of Case 2 turbid waters. It can be raised as well above highly reflective coccolithophorid blooms or above any other target that would exhibit a significantly enhanced reflectance at 560 nm.

The test uses a lookup table of the reflectance threshold, because this threshold is a function of geometry (when expressed in terms of the "MERIS reflectance", i.e., $\rho_w = \pi L_w/E_d(0^+)$).

This technique has been proposed initially by *[Bricaud and Morel, 1987]* for processing of the CZCS observations. It has been recently re-examined by *[Morel and Gentili, 2008]*, after the possible interference with residual, uncorrected, glint was identified in MERIS products. Another problem was identified in the MERIS data issued from the 2nd reprocessing, with too low values of the threshold for low Chl and large scattering angles (Figure 27). The flag was accordingly erroneously raised in clear Case 1 waters.

The solution adopted for the third reprocessing consisted in adding a constant reflectance value (0.0035) to the threshold extracted from the initial lookup table (see in *[Morel and Gentili, 2008]*). The 0.0035 value is expressed in terms of irradiance reflectance, and has to be converted into a directional reflectance before being added to the threshold from the lookup table ρ_wLUT(560), as follows:

Modified threshold = ρ_wLUT(560) + (0.0035 x πx$\mathcal{R}$/Q)

With Q ~4 and $\mathcal{R}$= 0.53, the correction becomes

Modified threshold = ρ_wLUT(560) + 0.00146

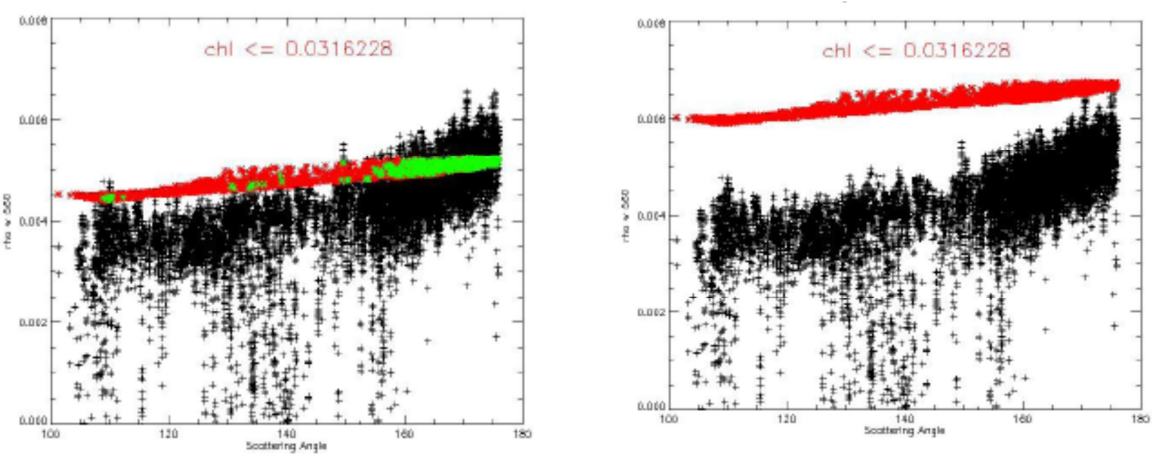

Figure 27: An example of the behaviour of the threshold used to set the case2anom flag from the 2nd (left) and 3rd (right) MERIS reprocessing. The black crosses are ρ_w(560) values from a transect across a MERIS scene when Chl< ~0.03 mg m^{-3}, and the red and green dots are the ρ_{wLUT}(560) values from the lookup table. With the 2nd reprocessing (left panel), the threshold was too low so clear Case 1 waters were identified as turbid waters for large scattering angles (> ~150°). This problem is solved with the 3rd reprocessing by adding a constant value to the threshold (right panel).

Impact, expected change on product

Increasing the threshold clearly overcomes the issue of erroneously identified pixels in the backscattering geometry (Figure 27). The expected change is a drastic decrease of the number of pixels belonging to the Case 1 water category that are erroneously identified as Case 2 turbid waters, in the Case2anom sense. This is illustrated on Figure 28. The results from the 3rd reprocessing clearly show turbid Case 2 waters where they should appear.

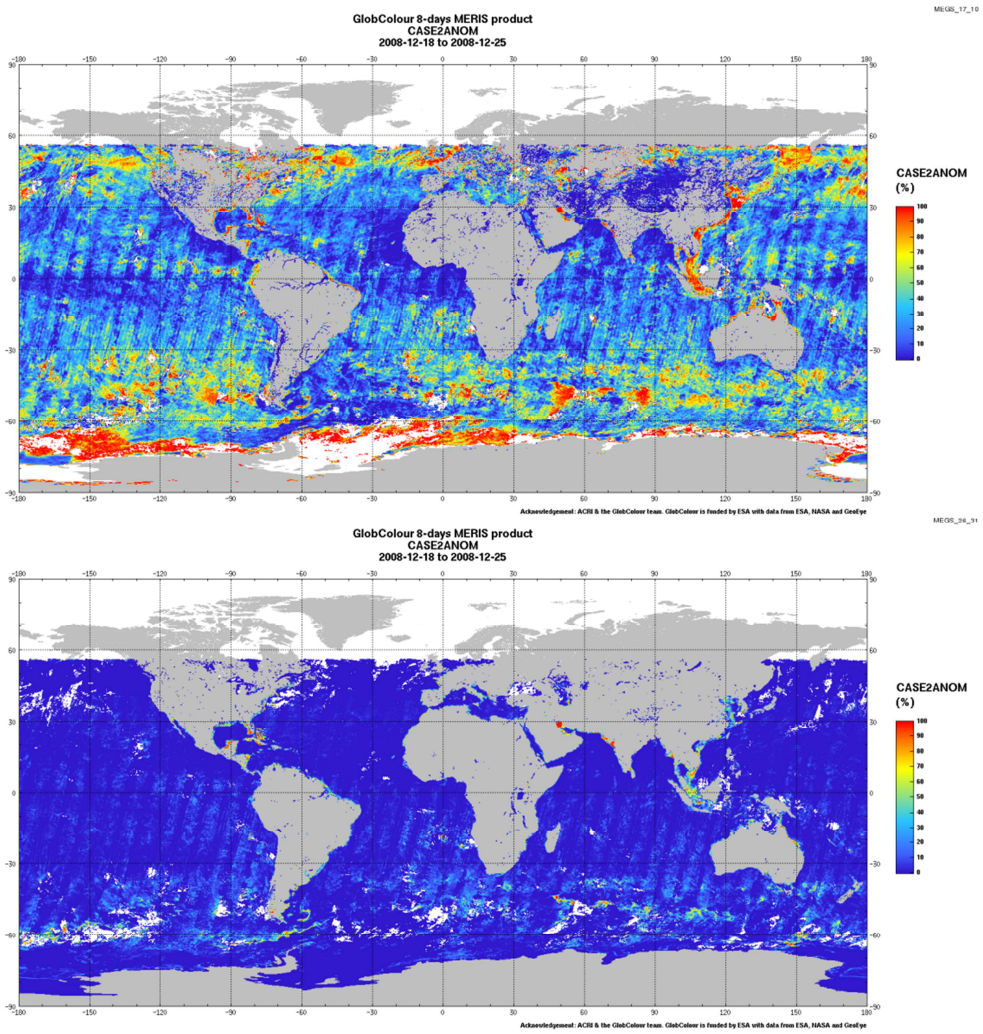

Figure 28: Global 8-day composite of the Case2anom flag from the 2nd (top) and 3rd (bottom) reprocessing.

References

Bricaud, A., and A. Morel, 1987. Atmospheric corrections and interpretation of marine radiances in CZCS imagery: use of a reflectance model. OceanologicaActa, N°SP, 33-50.

Morel, A. and B. Gentilli, 2008. Practical application of the “turbid water” flag in ocean color imagery: Interference with sun-glint contaminated pixels in open ocean. Remote Sensing of Environment, 112/3, 934-938.

6.8.4 Flag PCD_1_13

Contributors: Christophe Lerebourg (ACRI-ST), Constant Mazeran (ACRI-ST)

Purpose and description of changes

PCD_1_13 is a confidence flag for the thirteen water-leaving reflectances, which in particular test their positivity (see section 10 of the DPM for more information on PCD building from internal flags). After implementation of vicarious adjustment, it is observed as expected that the water leaving reflectances at longest wavelength are closest to zero for clear waters but sometimes slightly negative. This is interpreted as a noise around a virtually null reflectance. For this reason, the 3rd reprocessing introduces now a negative tolerance threshold.

The threshold at each wavelength relies on ideal remote-sensing reflectance to estimate the inherent variability of the signal and determine realistic noise level. Practically, time series over extremely clear and homogeneous oceanic waters (South Indian Ocean and South Pacific Gyre) have been used to compute variability of reflectance over 5x5 pixels windows. Because the inter-pixel noise does not follow a Gaussian distribution, it has been decided to consider the amplitude (difference between maximum and minimum in the window) rather than the standard deviation. The final threshold is equal to the 90 percentile of the amplitude distribution (see Figure 29).

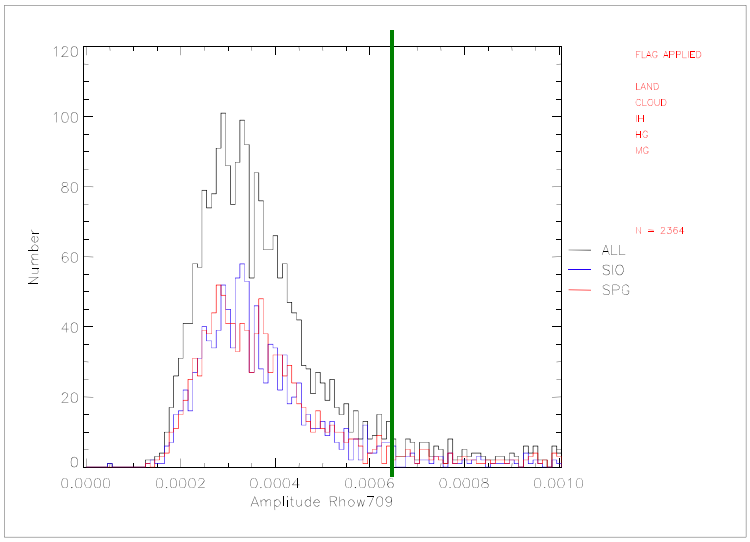

Figure 29 : Amplitude histogram at 709nm; the green line represent the 90 percentile

Impact, expected change on product

The thresholds are listed in Table 11 and are now included in the « Level 2 control parameter » ADF.

Table 11 : Thresholds to raise negative reflectance flag

Band	412	443	490	510	560	620	665	681	709
Threshold	-0.0058	-0.0046	-0.0029	-0.0024	-0.0017	-0.0012	-0.00083	-0.00071	-0.00065

As illustrated on Figure 30, the coverage of PCD_1_13 when including this tolerance threshold and vicarious adjustment is quasi similar to the one's without threshold (strict negativity) and without vicarious adjustment.

Note that although the thresholds have been computed on water leaving reflectances, the test is performed on the TOA water reflectante (t_u*t_d*ρw) and is slightly more tolerant.

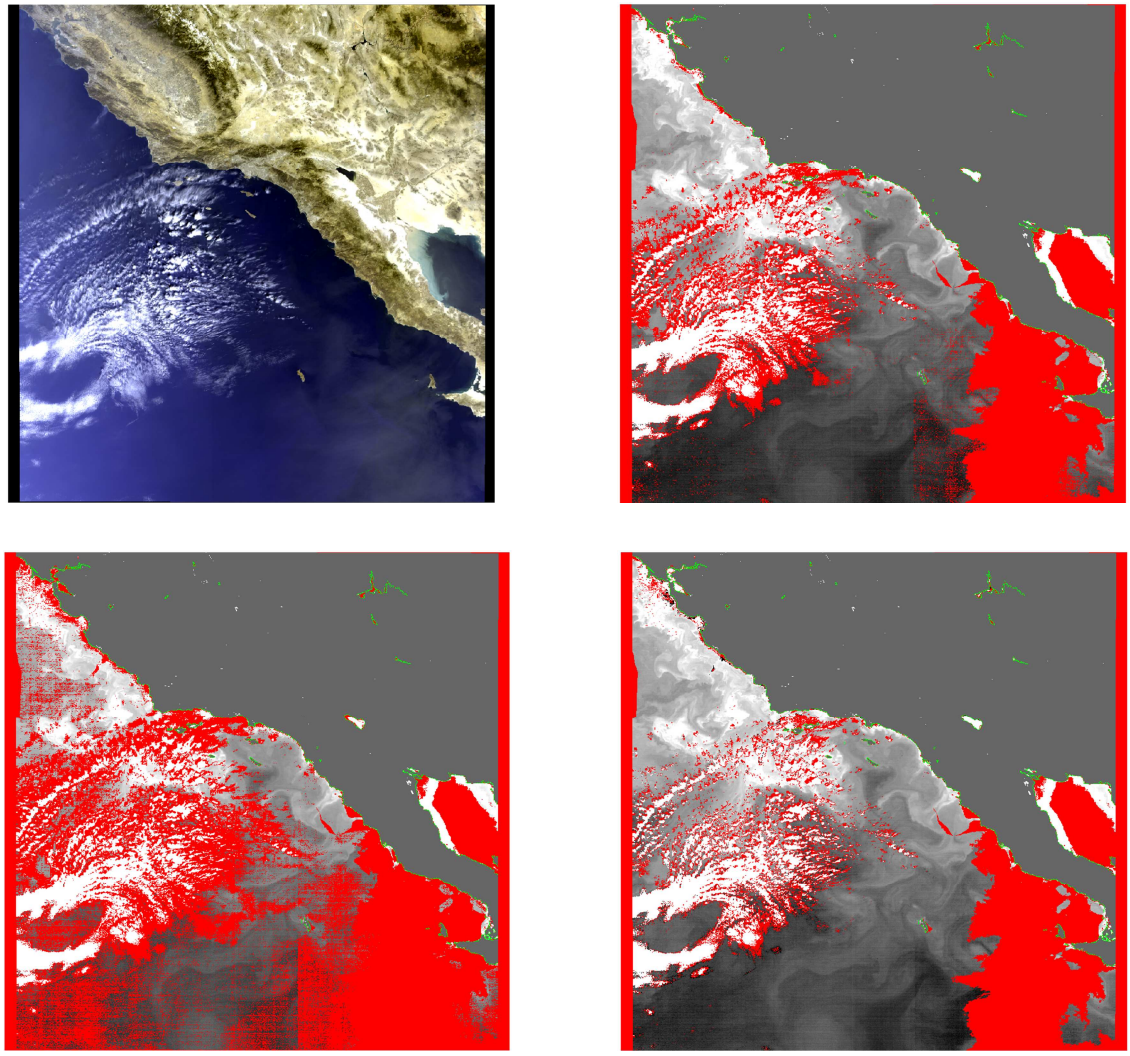

Figure 30: Example of flag PCD_1_13 over Gulf of California. Top left: colour composite of Level1; Top right: flag when no vicarious and no threshold; Bottom left: flag when vicarious and no threshold; Bottom right: flag when vicarious and threshold. Note the East part of the image is contaminated by glint.

Eventually, it is worth noting that PCD_1_13 is impacted by other changes, e.g. CASE2_ANOM.

6.8.5 Flag PCD_16 and PCD_17

Contributor: Roland Doerffer (HZG)

Purpose and description of changes

Due to the new atmospheric correction procedure for case 2 water, the algorithms for the flagsPCD_16/17 had to be changed. It is now triggered by one of the following cases:

- The TOA reflectance spectrum is out of scope of the training data set for training the atmospheric correction neural network;
- The water leaving reflectance spectrum is out of scope of the training data set for determining the water leaving radiance reflectance;
- The output of the water neural network is close to the minimum or maximum value of the IOPs used for training the network. This is to indicate that the true value can be below or above the output value of the neural network.

Since only 1 bit was reserved for flagging all case 2 water products, these three flags have to be combined using logical *or*, which triggers PCD_16/17. Consequence is that the cause for triggering the flag cannot be determined by the user.

Details of the three conditions for the flag:

- TOA reflectance spectrum is out of scope: For the identification of Top Of Atmosphere reflectance spectra, which are out of scope of the training range, an auto-associative neural network is used. This network has the 12 TOA reflectance spectral bands as input and output. The middle hidden layer is used as a bottleneck layer, the number of neurons of which defines the information content of the training data set. Reflectance spectra, which are out of scope produce output spectra, which deviate from the input spectra. The RMS deviation using all bands determines the out of scope error. If this value is above a defined threshold the PCD_16/17 is triggered;
- Water reflectance spectrum is out of scope: For this test the combination of an inverse and forward neural network is used as it was the case in all MEGS version before.

Impact, expected change on product

Due to the new atmospheric correction procedure the triggering of flags due to errors in the water leaving reflectances should be significantly reduced and thus more pixels in case 2 waters and under sun glint should be usable.

Known issues:

The threshold for triggering the PCD_16/17 is too relaxed, hence the PCDs are almost never raised.

7 Level 2 data processing – Land branch

7.1 Water vapour over land

Contributors: Jürgen Fischer (FUB)

Purpose and description of changes

The impact of the spectral slope of the surface albedo has been neglected in the previous versions of MERIS water vapour retrieval. Since sensitivity studies and global observations of the spectral surface albedo show that the spectral slope is significant, an improvement of the current algorithm has been envisaged.

The new algorithm for the retrieval of atmospheric water vapour over cloud free land surfaces is based on the inversion of the radiative transfer in the atmosphere by using an artificial neural network, while the previous procedure was based on a regression. The required radiative transfer simulations have been performed with the radiative transfer code MOMO [*Fell and Fischer, 2001*]. The new algorithm accounts for the impact of the spectral variability of the surface reflectance by using MERIS Albedomap data or measurements at 779 nm and 865 nm when there is no saturation on both MERIS channels [*Leinweber and Fischer, 2011*].

Impact, expected change on product

The new water vapour product has a significantly smaller impact on the surface albedo and its spectral slope. A higher accuracy of the water vapour retrieval is expected as shown in first validation studies [*Leinweber and Fischer, 2011*]. An extensive validation of the new algorithm by a comparison of the retrieved MERIS water vapour concentrations to ground based water vapour measurements was performed. Ground based water vapour measurements come from the Microwave Radiometers (MWR) of the ARM-SGP site in Oklahoma/USA, the Global Positioning System (GPS) stations in Germany and Radio soundings over central Europe. A high agreement between MWR and GPS total water vapour retrievals is found. The root mean square deviation is 1.40 mm (bias is -0.03mm) for MWR data, 1.22mm (bias is 0.97mm) for GPS, and 2.28mm (bias=1.63mm) for Radio sounding measurements. This investigation shows that the accuracy of the new water vapour algorithm has been significantly improved.

References

R. Leinweber and J. Fischer, 2011: Water vapor retrieval from MERIS satellite measurements over cloud free land areas. Submitted to J. Appl. Met.

7.2 Land Aerosol Remote Sensing (LARS)

Contributors: Richard Santer (ULCO), Didier Ramon (HYGEOS), Ludovic Bourg (ACRI-ST)

Purpose and description of changes

Initial data processing: The initial algorithms

LARS (Land Aerosol Remote Sensing) aims to provide an aerosol product (Aerosol Optical Thickness at 440 nm and Angström Coefficient ε between 440 nm and 670 nm) over pixel covered by dense vegetation).

The first step is to identify these pixels after a standard Rayleigh correction through a spectral index: the ARVI. The initial algorithm [*Santer et al., 1999*, http://envisat.esa.int/instruments/meris/atbd/atbd_2_15.pdf] was conceived for Dense Dark Vegetation (DDV). For these DDV pixels, their bidirectional surface reflectance in B1, B2 and B7 were provided by first the albedo and second a BRDF model both derived from POLDER measurements. The coupling with the surface reflectance and the atmospheric scattering is described in [*Ramon and Santer, 2001*] and http://envisat.esa.int/instruments/meris/atbd/atbd_2_19.pdf. The basic aerosol retrieval was to use B1, B2 and B7 and to refer to 26 power laws, associated to α, as aerosol models with an assumed refractive index of 1.44 and no absorption. The three spectral bands were used to derive for each aerosol model three AOT values. A linear regression on these three AOTs gives α. The selected aerosol model offers the best agreement on α between the experimental and theoretical values. A theoretical error analysis was reported by [*Santer et al, 2003*].

This first version of the algorithm was implemented for the 1st processing. The first evaluation [*Ramon et al, 2003*] pointed out the poor quality of the α retrieval. Therefore, for the first processing, in order to secure the AOT at 440 nm, the retrieval of the AOT assumed α equal to -1.

2nd reprocessing change: The initial LUTs

In order to improve the spatial coverage of the aerosol product, the concept of DDV was extended to "less" dark vegetation, the so-called LARS pixels [*Borde et al, 2003*]. The reflectance of the LARS is a linear law versus the ARVI [*Santer et al, 2007*]. The linear fit being conducted on the MODIS albedo map product to have at the end LUTs in B1, B2, B7 and B13 of the offset and of the slope of the LARS albedo. It is monthly LUTs by 1 degree latitude and 1 degree longitude.

3rd reprocessing changes: The two band retrieval and the new LUTs

The retrieval of the two parameters of the aerosol product requires using two spectral bands. We tested different options ending by (B2-B7) for implementation.

The MERIS Albedo Map project (http://www.brockmann-consult.de/albedomap/) offers the opportunity to regenerate a new set of LUTs for the LARS reflectance with:

- A perfect spectral matching.
- An improved spatio-temporal coverage.

A comprehensive summary of the aerosol retrieval algorithm over land including up to date changes has been recently released [*Ramon et Santer, 2011*]

Impact, expected change on product

- From the new pixel classification: The new flagging of the cirrus clouds is an important step in the quality of the aerosol retrieval;
- From the new LUTs: The new LARS reflectance LUT's should improve the aerosol retrieval spatial cover. We expect an improvement of the aerosol Angström exponent retrieval;
- From the two band retrieval: The processing speed should increase without loss of accuracy as the 412 nm channel additional information concerning aerosol scattering is very small.

Known issues:

There are still serious limitations:

- The BRDF of the LARS is only valid for the DDV. A BRDF LUT needs to be generated for different LARS albedo values;
- A daily L3 has to be generated as a reference aerosol product.

References

BORDE R., RAMON D., Schmechtig C., Santer R.(2003) Extension of the DDV concept to retrieve aerosol properties over land from the Modular Optoelectronic Scanner sensor. International Journal of Remote Sensing, vol 24, No 7, 1439-1467.

RAMON D, SANTER R. (2001) "Operational remote sensing of aerosols over land to account for directional effects." Applied Optics, Vol 40 (18): 3060

RAMON D., SANTER R. AND VIDOT J. (2003).First validation of MERIS aerosol product over land.Envisat Validation Workshop, 9-13 December 2002 ESRIN, Frascati,Italy Proceedings on CD rom.

SANTER R., CARRERE V., DUBUISSON P., & ROGER J.C. (1999). Atmospheric correction over land for MERIS, International Journal of Remote Sensing, Vol. 20. Issue 9, p 1819-1840.

SANTER R., ZAGOLSKI F., RAMON D., FISCHER J., DUBUISSON P., (2005) Uncertainties in Radiative Transfer Computations, Consequences on the MERIS products over land. International Journal of Remote Sensing,.International Journal of Remote Sensing. Vol. 26, No. 20, 20 October 2005, 4597–4626

SANTER R., RAMON D., VIDOT J., DILLIGEARD E., (2007). A Surface Reflectance Model for Aerosol Remote Sensing over Land.International Journal of Remote Sensing.Vol 28.no3-4, pp. 737-760.

Schmechtig C., CARRERE V., DUBUISSON P., ROGER J.-C. and Santer R.(2003). Sensitivity analysis for the aerosol retrieval over land for MERIS .International Journal of Remote Sensing, Vol 24, No14, 2921-2944.

Applicable Document

Ramon D. and R. Santer, MERIS ATBD 2.15 - Land Aerosol Remote Sensing – Version 2011

7.3 Surface Pressure

Contributors: Jürgen Fischer (FUB)

Purpose and description of changes

The 2nd MERIS processing used to derive prominent camera boundaries along the MERIS swath with surface pressure jumps up to 100 hPa. In the case of MERIS measurements in the O2 A-band, one of the largest sources of error is the instrumental stray light [*Lindstrot et al. 2009*]. An empirical stray light correction has been derived from a new surface pressure algorithm, a digital height model and the use of ECMWF surface pressure values [*Lindstrot et al., 2010*].

The new surface pressure algorithm is based on numerous radiative transfer simulations [MOMO, *Fell and Fischer, 2001*], covering combinations of all relevant parameters within the natural variability. However, the temperature profile, which has an impact on the absorption line within the O2 A-band, is assumed to be constant, knowing that this still leads to uncertainties. Artificial neural networks have proven to be suitable tools to perform the multi-dimensional non-linear regression relating the measured radiance to the surface pressure.

The accuracy of the new surface pressure algorithm has been found to be within 10 hPa above ice surfaces in Greenland and 15 hPa above desert and mountain scenes in Northern Africa and Southwest Asia. In a case study above Greenland, the accuracy has been enhanced to be better than 3 hPa by spatial averaging over areas of 40 km * 40 km [*Lindstrot et al., 2009*].

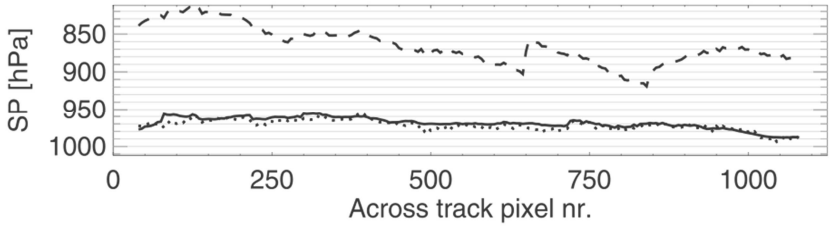

Figure 31: Along-track median values of surface pressure derived from DEM (solid lines) and MERIS spectral campaign measurements before (dashed) and after (dotted) optimization [Lindstrot et al, 2009].

Impact, expected change on product

Significant reduction of camera boundary jumps and a more accurate surface pressure along the full MERIS swath is achieved. The surface pressure product is more consistent and accurate in the 3rd reprocessing.

References

Lindstrot, R., R. Preusker, and J. Fischer, 2009: The retrieval of land surface pressure from MERIS measurements in the oxygen A band. J. Atmos. Oceanic Technol., 26, 1367–1377.

Lindstrot, R, Preusker, R. and Fischer, J., 2009: Remote Sensing of Multilayer Cloud-Top Pressure Using Combined Measurements of MERIS and AATSR Onboard ENVISAT. J. Appl. Meteor. Climatol., 49, 1191-1204.

Lindstrot, R., R. Preusker, and J. Fischer, 2010: Empirical Correction of Stray Light within the MERIS Oxygen A-Band Channel. Atmos. Oceanic Technol., 27, 1185–1194.

7.4 FAPAR (rectified reflectance - MGVI)

Contributors: Ludovic Bourg (ACRI-ST)

Purpose and description of changes

The change introduced in the MGVI (MERIS Global Vegetation Index) algorithm do not impact the index itself (FAPAR value) but the accompanying "rectified reflectance" products: computation of these products have been extended to non vegetated Land surfaces, for which FAPAR computation is not relevant, thanks to dedicated set of retrieval parameters. Wherever the algorithm detects non vegetated bright soils through spectral tests, the dedicated set of retrieval parameters is used to compute rectified reflectance. A backward loop has also been added to allow re-classification and (re-)processing of pixels firstly classified as "vegetated" but yielding to negative FAPAR as "bright" surfaces with appropriately computed rectified reflectance.

Impact, expected change on product

No impact on FAPAR, or on rectified reflectance where FAPAR retrieval succeeds (assuming same Level 1b input, i.e. not accounting for calibration changes discussed in section 3.1).

Marginal impact on rectified reflectance for pixels over which FAPAR retrieval fails (marginal in terms of number of affected pixels, can bring significant changes to rectified reflectance products).

Rectified reflectance provided over "bright soil" pixels (not identified as snow or ice covered).

References

MERIS Vegetation Index ATBD 2.10 – Version 2011

7.5 Flag Snow

Contributors: Carsten Brockmann (Brockmann Consult)

Purpose and description of changes

A test for snow and ice using the MERIS Differential Snow Index (MDSI, *Brockmann and Krüger 2010*) has been introduced in the pixel classification processing step (see section 4.2.3). Over land this test identifies snow covered land surfaces when the brightness exceeds certain thresholds and the MDSI separates the spectrum from that of a cloud due to the slightly stronger absorption of snow in the NIR as compared to clouds.

In the 3rd reprocessing, the result of this test has been introduced as a new flag into the Level 2 product.

Impact, expected change on product

The Snow_Ice flag is included in the flags MDS of the MERIS L2 product for land pixels. It is stored in bit 8, which was not used over land in 2nd reprocessing. Over water, this bit was and is used for the Case2_S flag.

BEAM 4.9 supports the new flag coding. It is available from the BEAM download Website (http://www.brockmann-consult.de/cms/web/beam/software).

References

Brockmann, C., Krüger, O. (2010) Snow Radiance Cloud Snow Ice Identification ATBD. Available on http://www.brockmann-consult.de/cms/web/beam/forum/-/message_boards/message/52330

End of document